PHYSICAL REVIEW D VOLUME 43, NUMBER 6 15 MARCH 1991

Quenched spectrum with staggered fermions

Rajan Gupta
T-8, MS-B285, Los Alamos National Laboratory, Los Alamos, New Mexico 87545

Gerald Guralnik
Physics Department, Brown University, Providence, Rhode Island 02912

Gregory W. Kilcup
Physics Department, The Ohio State University, Columbus, Ohio 43210

Stephen R. Sharpe
Institute for Theoretical Physics, University of California, Santa Barbara, California 93106
*and Physics Department, University of Washington, Seattle, Washington 98195**
(Received 19 October 1990)

We present results for the spectrum of QCD in the quenched approximation using staggered fermions at $\beta=5.7$, 6.0, and 6.2. We use extended wall sources, which give a better projection onto the ground state, and allow us to study many nonlocal pion and ρ states, as well as the Δ baryon. Staggered flavor-symmetry breaking reduces dramatically from $\beta=5.7$ to 6.2. For $\beta=6$, the ratio m_N/m_ρ lies significantly below 1.5 for $m_q<m_s$. At $\beta=6$ we study finite-volume effects using $16^3\times 40$ and $24^3\times 40$ lattices. We reanalyze our old data at $\beta=6.2$ and resolve the problem of the anomalously light scalar state.

I. INTRODUCTION

In this paper we present results for the hadron spectrum in the quenched approximation using staggered fermions. Pinning down the quenched spectrum is an important step in the program of using lattice calculations to extract physically useful quantities. If we cannot extract the masses of the lightest few states with small errors, and make reliable extrapolations to zero quark mass, then calculations of more complicated quantities are suspect. Furthermore, we would like to know how well the quenched approximation reproduces the physical spectrum, for this gives us some indication of the trustworthiness of other quenched calculations.

We are keenly aware of these points because our spectrum calculation is being done as part of a project to evaluate weak matrix elements.[1] We have tried, therefore, to understand the errors due to (a) finite lattice spacing, (b) finite lattice size, (c) extrapolations from large quark masses, and (d) the lack of an asymptotic signal in hadron correlators due to a poor choice of operators. These are the major problems afflicting quenched calculations, including our previous work.[2] We can address these points since (a) we have results at three lattice spacings ($\beta=5.7,6.0,6.2$), (b) we have lattices of sizes $16^3\times 40$ and $24^3\times 40$ at $\beta=6$, (c) we work with very low quark masses at $\beta=5.7$, and (d) at $\beta=6.2$ we can compare our present results using extended operators with those of our previous work which used point sources.[2] Through a combination of better methods and greater computer resources we are able to improve our understanding of these issues. We are, however, far from providing definitive answers.

The major technical innovation of this work lies in the nature of our extended sources and operators. In the first part of this paper (Secs. II–IV) we explain these sources, the states that they create, and the operators we use to destroy the states.

Following this we turn to numerical details. In Sec. V we explain our fitting procedure. This is much improved over our previous methods,[2] and brings us up to the state of the art.[3] We now use the full covariance matrix to do fits, and make extensive use of effective mass plots to determine their reliability. We have reanalyzed our old data,[2] finding substantial changes for the baryon masses, and that the previously claimed signals in positive-parity meson channels are unreliable.

Section VI gives the parameters of the simulations, and is followed in Secs. VII–IX by our results for the spectrum, together with a comparison with previous work. We discuss, in turn, results from $16^3\times 32$ lattices at $\beta=5.7$, $16^3\times 40$ and $24^3\times 40$ lattices at $\beta=6.0$, and $18^3\times 42$ lattices at $\beta=6.2$. Section X discusses chiral quantities ($\langle\bar\chi\chi\rangle$, f_π) and the lattice spacing. Finally, Sec. XI gives an overview of all our results, and our conclusions.

We have concentrated entirely on staggered fermions in this project. Results with Wilson fermions have also improved substantially over the last year or so. For a comprehensive review of the present status of all quenched spectrum calculations, see Ref. 4.

Preliminary accounts of part of this work have also been given in Refs. 5 and 6.

II. REPRESENTATION OF STAGGERED STATES AT ZERO SPATIAL MOMENTUM

For staggered fermions, the SU(4)-flavor symmetry is only recovered in the continuum limit; the symmetry

 ©1991 The American Physical Society

group for finite lattice spacing is smaller.[7,8] In the continuum limit, mesons lie in the SU(4) representations 1 and 15, while on the lattice these representations break into many smaller ones. For example, the continuum 15-plet of pions breaks into seven lattice representations [four three dimensional (3D) and three 1D], and the ρ 15-plet (times three spin components) breaks into eleven representations (four 6D and seven 3D). For baryons, the two ground-state 20's break into combinations of the three lattice representations, the 8, 8′, and 16.[9] In these examples we have assumed, as is the case throughout this paper, that the states are at zero spatial momentum. We would like to calculate the masses of as many of these lattice representations as possible in order to test the approach to the continuum limit. Almost all previous calculations, however, have studied only those states that can be created with completely local operators. This allows one to study two of the 1D pion representations, two of the 3D ρ representations, and only one baryon representation (the 8). The exceptions are Ref. 10, which studied, in SU(2) gauge theory, the same set of pion representations as we consider in this paper, and our previous work,[2] which considered a few nonlocal pion and ρ representations.

To label the states we use the notation of Ref. 11, which is less precise than that of Ref. 7, but is simpler. We comment on the lack of precision at the end of this section. Particles are denoted by $\Gamma_S \otimes \Gamma_F$, where the first Γ matrix labels the spin of the bilinear which creates the state, and the second labels the SU(4) flavor. Γ_S and Γ_F are elements of the Euclidean Clifford algebra, and are labeled by four-vectors (S and F) whose elements are defined mod2. For example, if $S=(S_1S_2S_3S_4)$, then $\Gamma_S=\gamma_1^{S_1}\gamma_2^{S_2}\gamma_3^{S_3}\gamma_4^{S_4}$. In this notation, the continuum pion representations break down as

$$\begin{aligned} 15 \rightarrow & (\gamma_5\otimes\gamma_i)\oplus(\gamma_5\otimes\gamma_i\gamma_4)\oplus(\gamma_5\otimes\gamma_i\gamma_5)\oplus(\gamma_5\otimes\gamma_i\gamma_4\gamma_5) \\ & \oplus(\gamma_5\otimes\gamma_4)\oplus(\gamma_5\otimes\gamma_5)\oplus(\gamma_5\otimes\gamma_4\gamma_5) , \\ 1 \rightarrow & (\gamma_5\otimes 1) . \end{aligned} \tag{2.1}$$

In the first line, $i=1,2,3$, so the representations are three dimensional. The other representations are one dimensional. The continuum ρ's become

$$\begin{aligned} 15 \rightarrow & (\gamma_i\otimes\gamma_j)\oplus(\gamma_i\otimes\gamma_j\gamma_4)\oplus(\gamma_i\otimes\gamma_j\gamma_5)\oplus(\gamma_i\otimes\gamma_j\gamma_4\gamma_5) \\ & \oplus(\gamma_1\otimes\gamma_i)\oplus(\gamma_i\oplus\gamma_i\gamma_4)\oplus(\gamma_i\otimes\gamma_i\gamma_5)\oplus(\gamma_i\otimes\gamma_i\gamma_4\gamma_5) \\ & \otimes(\gamma_i\otimes\gamma_4)\oplus(\gamma_i\otimes\gamma_5)\oplus(\gamma_i\otimes\gamma_4\gamma_5) , \\ 1 \rightarrow & (\gamma_i\otimes 1) . \end{aligned} \tag{2.2}$$

On the first line, $i\neq j$, so the representations are six dimensional, while all others are three dimensional.

To construct operators which create states in these various representations, we use extended quark fields

$$q(t,\eta)=\sum_{\mathbf{y}}\chi[(2\mathbf{y},t)+\eta] . \tag{2.3}$$

In this equation, and in the following, η is a four-vector whose components are defined mod2, and which thus points to a position in a 2^4 hypercube. The extended quark fields are labeled by η, and by the time t. In fact, the time plays no role in the following discussion, and we will drop it henceforth. We do not include gauge links in our definition of extended fields, but assume that the lattice has been fixed to either the Coulomb or Landau gauge, as discussed in the following section.

In terms of these extended fields, the operator which creates the state $\Gamma_S\otimes\Gamma_F$ is

$$\mathcal{O}_{S,F}=\sum_{\eta,\eta'}\bar{q}(\eta)q(\eta')\mathrm{Tr}(\Gamma_\eta^\dagger\Gamma_S\Gamma_{\eta'}\Gamma_F^\dagger) . \tag{2.4}$$

The trace picks out terms in which there is definite distance between the quark and antiquark field. If $S={}_2F+\delta$, where δ is another hypercube vector, then all nonzero terms in Eq. (2.4) have $\eta={}_2\eta'+\delta$. We call the number of links between η and η' the "distance" of the operator. Clearly operators of distances zero to four are possible. The standard local operators pick out the distance zero states, i.e., those in which $S=F$.

It might be helpful to list the local states in the notation we are using, and compare to the traditional notation. The latter is collected in Appendix A of Ref. 12. The Goldstone pion, which we call the π, is in the 1D representation $\gamma_5\otimes\gamma_5$, which is labeled PS in Ref. 12. The other local pion is the $\tilde{\pi}$, which is in the 1D representation $\gamma_4\gamma_5\otimes\gamma_4\gamma_5$, and is in the SC channel. Relative to the local pion, the operator which creates it has the phase $(-1)^{x+y+z}$. The two local ρ's are in the 3D representations $\gamma_i\otimes\gamma_i$ and $\gamma_4\gamma_i\otimes\gamma_4\gamma_i$. The former lie in the VT channel [with phases $(-1)^{x_i}$ relative to the π], the latter in the PV channel [with phases $(-1)^{x_j+x_k}$ where j and k are different from i].

As mentioned above, the description we have given is slightly incorrect. There are two related problems. The first is a trivial over-counting: the states $\gamma_4\Gamma_S\otimes\Gamma_F$ and $\Gamma_S\otimes\Gamma_F$ are the same. The corresponding operators couple to the same states. This is clearly true in the continuum limit, but also holds at finite lattice spacing. it means that we can always take δ_4 (the Euclidean time component of δ) to vanish, though in actual calculations operators with $\delta_4=1$ often give better signals. We refer to operators with $\delta_4=1$ as nonlocal in time (NLT), and use LT to denote operators with $\delta_4=0$.

The second problem is more important. It is not, in fact, possible to make an operator which projects onto a single state.[9] The operator $\mathcal{O}_{S,F}$ couples to both $\Gamma_S\otimes\Gamma_F$ and $\gamma_4\gamma_5\Gamma_S\otimes\gamma_4\gamma_5\Gamma_F$. The point is that the operators corresponding to these two states have the same relative phase on a given time slice, but different relative phases between adjacent time slices. One state is "oscillating" in time [$\propto(-1)^t\exp(-M|t|)$] while the other is smooth. Without knowledge of the masses, one cannot project against one or other state exactly. It is true, however, that the coupling of the state $\gamma_4\gamma_5\Gamma_S\otimes\gamma_4\gamma_5\Gamma_F$ to $\mathcal{O}_{S,F}$ is suppressed by $\tan(M)$, and vanishes in the continuum limit.

III. WALL SOURCES

One of the major problems facing spectrum calculations is the need to extract a clear asymptotic signal. If we consider a state at zero spatial momentum (which is the case throughout this paper) then the Euclidean correlator falls as $\exp(-M|t|)$ for large time separations, M being the mass of the state. The goal is to have a strong signal at large separations in order to remove contamination from excited states while keeping statistical errors small.

This has been a particularly difficult problem for the calculation of baryon masses. The Tsukuba group[13] have argued that one needs lattices which are extremely long in the time direction so that signals can be followed out for many time slices. They have shown that, as one goes to smaller quark masses, one can extract a baryon mass which is significantly different from the correct value if too short a lattice is used.

A more economical solution to this problem is to use better operators to create and destroy the state. If one can enhance the overlap with the lightest particle compared to that of the excited states, then one will see the asymptotic signal at smaller time separations. Since present calculations are done with a lattice spacing $a \sim 0.1$ fm, while hadrons have typical radii of ≥ 0.5 fm, it seems likely that extended operators would improve the signals. In the last few years there has been a flurry of effort aimed at finding the best such source, building upon the original idea of Ref. 14. For a general discussion of source methods, see Ref. 15. Our choice was driven by the needs of our matrix element calculation, for which we require that the meson states have zero spatial momenta. The simplest way to arrange this is to make the quark source have zero spatial momentum, i.e., to spread it out uniformly over an entire time slice. This choice we call a wall source.[6]

An important issue is how we make the source gauge invariant. We do this by fixing the source time slice to the Coulomb gauge, the same method as has been advocated by the APE group.[16] This gauge has no ghosts, so that nonlocal operators produce only the physical mesons and baryons. By accident we left the source time slice in the Landau gauge on a subset of our lattices at $\beta=6$. The physical interpretation of the results in the Landau gauge is unclear. The process of gauge fixing propagates information across time slices, so that wall source operators are, in some sense, spread out over all time. Thus correlation functions of two extended operators contain a component in which the two sources overlap, for which there is no interpretation as a state being propagated by the Hamiltonian. In order for the Landau gauge results to make sense, the overlapping components must be small at long times. This appears to be true, for there is little difference between the masses extracted from two-point functions in the two gauges. In fact, there is little difference in the form of the correlators even at short times.

A related problem is that there may be disconnected components in correlation functions of extended Landau gauge operators. In the Landau gauge there is a nonvanishing quark propagator, and numerical studies indicate that the quark propagator falls exponentially at long times, so that one can extract a quark mass m_Q.[17] The disconnected component consists of separate quark and antiquark propagators, with lowest energy $2m_Q$. If this unphysical component is lighter than the meson in the channel under consideration, then the analysis would become very difficult. In fact we find that $m_\rho < 2m_Q$ and $m_N < 3m_Q$ for our range of quark masses. Thus it is not surprising that we also find that m_π, m_ρ, and m_N from the Landau and Coulomb gauge sources agree well.

A quark source at zero spatial momentum is a linear combination of the extended quarks fields of Eq. (2.3), which are labeled by the hypercube four-vector η. We restrict our fields to a single time slice, i.e., $\eta_4=0$, so that the most general zero-momentum source is a linear combination of eight extended quark fields: $S=\sum_\eta \mathcal{A}(\eta) q(\eta)$. A wall source propagator is thus determined by

$$(\not{D}+m)_{ab} G(x)_b = \delta_{ac}\delta(t,t_s) \sum_{\mathbf{y}} \sum_{\eta} \mathcal{A}(\eta)\delta(\mathbf{x},2\mathbf{y}+\eta) , \tag{3.1}$$

where $x=(\mathbf{x},t)$, t_s is the source time slice, and c is its color. $\not{D}$ is the standard staggered fermion action given, for example, in Ref. 2. Note that we use lattices with even dimensions, and use periodic boundary conditions in the spatial directions.

For a given choice of amplitudes $\mathcal{A}(\eta)$, the mesons and baryons that are created by combining the propagators G are a subset of the total available states. Motivated by matrix element calculations we use two sources, which we call *even* and *odd*. The former is defined by $\mathcal{A}(\eta)=1$ for all η, the latter by $\mathcal{A}(\eta)=(-1)^{\eta_x+\eta_y+\eta_z}$. Both are nonzero for every point on the time slice. We refer to the propagator from an *odd* source as an o, and that from an *even* source as a q. With these types of propagators we can consider four types of mesons: qq, oo, qo, and oq. Here the first letter refers to the antiquark propagator, the second to the quark. We use a similar notation for the baryons.

To explain why we choose these particular wall sources, we must first explain which states they create. Combining extended quark and antiquark fields gives a sum of operators of the form of $\mathcal{O}_{S,F}$ in Eq. (2.4). To determine which states are created we have to find the operators which appear in this sum. Since the wall sources are contained only on a single time slice, we know that $S_4=F_4$. This is not a restriction on the states, however, as explained above. We also know that the states must come in pairs, for we have that

$$\sum_{\substack{\eta,\eta' \\ \eta_4=\eta_4'=0}} \bar{q}(\eta) q(\eta') \mathrm{Tr}(\Gamma_\eta^\dagger \Gamma_S \Gamma_{\eta'} \Gamma_F^\dagger) = \tfrac{1}{2}(\mathcal{O}_{S,F} + \mathcal{O}_{S',F'}) , \tag{3.2}$$

where $\Gamma_{S'}=\gamma_4\gamma_5\Gamma_S$ and $\Gamma_{F'}=\gamma_4\gamma_5\Gamma_F$. This is the familiar result for staggered fermions that a single time-slice operator always produces two states, one of which oscil-

lates in time. For example, all pions ($S=\gamma_5$) are partnered with scalars ($S=\gamma_4$). In fact, as mentioned above, we cannot project out one of these states using a two time-slice operator, although we can suppress one of the amplitudes. With a single time-slice operator there is no suppression whatsoever.

To proceed further we must consider particular examples. We begin with the qq source, which can be written as

$$S_{qq}=\sum_{\delta}\sum_{\eta}\bar{q}(\eta)(-1)^{\eta_1+\eta_2+\eta_3}q(\eta+\delta)\ , \tag{3.3}$$

where the phase factor comes from the antiquark propagator. The oo source is similarly

$$S_{oo}=\sum_{\delta}(-1)^{\delta_1+\delta_2+\delta_3}\sum_{\eta}\bar{q}(\eta)(-1)^{\eta_1+\eta_2+\eta_3}q(\eta+\delta)\ . \tag{3.4}$$

These equations show that both sources are a sum of eight terms, one for each δ. Each of these terms is of the form of the left-hand side of Eq. (3.2), and thus creates two states. Both sources thus create the same 16 states, but with different amplitudes. States with "even" δ [i.e., $(-1)^{\delta_1+\delta_2+\delta_3}=1$] are produced with the same amplitude by both sources, while those with "odd" δ come with opposite amplitudes. Thus by forming $qq\pm oo$ we can select out one-half of the states. This filtering is essential for our weak matrix element calculation, and is the reason for our using o sources in addition to q sources.

To determine the representation of states that are created by the wall sources, we must find, for each δ, the choices of $\Gamma_S\otimes\Gamma_F$ with $S=F+\delta$ in which the traces in Eq. (3.2) give the alternating phase $(-1)^{\eta_1+\eta_2+\eta_3}$ appearing in Eqs. (3.3) and (3.4). This is a simple exercise, the result of which is given in Table I. The table also indicates which of the states couple to $qq+oo$ sources, and which to $qq-oo$. We have listed only the pion and ρ states; the accompanying scalars and axial vectors are obtained by multiplying both S and F by $\gamma_4\gamma_5$, as explained above.

The table also gives the results of a similar exercise for oq and qo sources. These can be written as

$$S_{oq}=\sum_{\delta}\sum_{\eta}\bar{q}(\eta)q(\eta+\delta) \tag{3.5}$$

and

$$S_{qo}=\sum_{\delta}(-1)^{\delta_1+\delta_2+\delta_3}\sum_{\eta}\bar{q}(\eta)q(\eta+\delta)\ , \tag{3.6}$$

respectively. The only difference from qq and oo sources is that the alternating phase is replaced by the identity.

In total, then, our sources create 32 states (including scalars and axial vectors), which we can organize into four sets of eight. The table shows the representations in which the pions and ρ's lie, and our labeling conventions. There are four pions, two in 1D reps, and two in 3D reps. The two 1D reps are the standard, local states. The π is the pseudo Goldstone pion, and we follow the notation of Ref. 2 and label the other pion $\tilde{\pi}$. The bonus from using our wall sources is two completely new 3D reps of pions with distance 1, which we label π_3 and $\tilde{\pi}_3$. In total we can study one-half the pion representations.

There are 12 different ρ's created by the wall sources. Of these, four lie in 3D reps, the other eight in 6D reps. The four 3D reps are different, and we label them arbitrarily as $A-D$. Some of the states in 6D reps are parts of the same representation, as must be true since there are only four 6D reps. There are three representatives each of ρ_6^A and ρ_6^B, while only one each of ρ_6^C and ρ_6^D. In total we have representatives of one-half of the 3D reps, and all the 6D reps. None of these ρ's are created by local operators, so that all of our ρ's are different from those usually studied.

To determine the baryons created by our wall sources, we use the work of Golterman and Smit.[9] To understand the following discussion, the reader must have in hand Table 3 of that work. Recall that there are only three baryon representations, the **8** (which contains the nucleon), the **8′** [in which the lightest state is the SU(4) analog of the $\Delta(1232)$], and the **16** (which also couples to the

TABLE I. Pion and ρ states created by the four wall sources $qq\pm oo$ and $qo\pm oq$. δ is the separation between quark and antiquark fields, as explained in the text. The column labeled "State" gives our notation for the particles, while "Dim." gives the dimension of the lattice representation in which the particles lie.

δ	$qq+oo$	State	Dim.	$qo+oq$	State	Dim.
000	$\gamma_5\otimes\gamma_5$	π	1	$\gamma_4\gamma_5\otimes\gamma_4\gamma_5$	$\tilde{\pi}$	1
011	$\gamma_3\otimes\gamma_2$	ρ_6^A	6	$\gamma_3\gamma_4\otimes\gamma_2\gamma_4$	ρ_6^B	6
101	$\gamma_1\gamma_4\otimes\gamma_3\gamma_4$	ρ_6^B	6	$\gamma_1\otimes\gamma_3$	ρ_6^A	6
110	$\gamma_2\otimes\gamma_1$	ρ_6^A	6	$\gamma_2\gamma_4\otimes\gamma_1\gamma_4$	ρ_6^B	6
	$qq-oo$			$qo-oq$		
001	$\gamma_5\otimes\gamma_5\gamma_3$	π_3	3	$\gamma_4\gamma_5\otimes\gamma_3\gamma_4\gamma_5$	$\tilde{\pi}_3$	3
010	$\gamma_3\otimes\gamma_1\gamma_4\gamma_5$	ρ_6^C	6	$\gamma_3\gamma_4\otimes\gamma_1\gamma_5$	ρ_6^D	6
100	$\gamma_1\gamma_4\otimes\gamma_4$	ρ_3^A	3	$\gamma_1\otimes 1$	ρ_3^B	3
111	$\gamma_2\otimes\gamma_2\gamma_4\gamma_5$	ρ_3^C	3	$\gamma_2\gamma_4\otimes\gamma_2\gamma_5$	ρ_3^D	3

nucleon). Only the **8** has been studied up to now, this being the representation produced by local operators. We are particularly interested in the **8′**, since the staggered fermion Δ has not been seen previously.

It turns out that all the possible combinations of three propagators, *qqq*, *qqo*, etc., create the same states, and we use only *qqq* and *ooo* in our calculations. These contain operators in which the three extended quark fields have all possible relative positions in the spatial cube. These operators divide up into classes which are labeled in Ref. 9. For example, class 1 operators are local, and class 2 operators have two quarks at one site and the third one link away. Each class of operator couples to different states depending on the relative signs of the different elements obtained from one another by translations, rotations, and reflections. Thus certain combinations of class 2 operators couple to the **8**, while other combinations couple to the **16**. As shown in Table 3 of Ref. 9, the latter combinations are "traceless" in the sense that the signs of various components add to zero. With our sources, however, the different components always come in with relative plus signs, and so our source contains class 2 operators which couple only to the **8** and not the **16**. By a similar analysis we find from Ref. 9 that our source has class 3 operators coupling to the **8**, class 4 coupling to the **8′**, classes 5 and 6 to the **8**, and finally class 7 to the **8′**. In addition, after correcting some sign errors in the results of Ref. 9, we find that our source also contains class 4 and 6 operators coupling to both the **8′** and to the **16**.

The upshot of all this is that our sources create states in all three baryon representations. As always, these representations come in both parities, so that we can in principle study six representations. In practice, the signal is poor for the negative-parity states, and we do not discuss them further.

In summary, our wall sources have a number of virtues relative to point sources. First, they are extended, which should improve the signal. Second, the states they create come from a larger number of distinct representations. This is a help when studying staggered flavor-symmetry restoration as we approach the continuum limit. Third, we can finally investigate the Δ using staggered fermions.

We can now explain our specific choice of wall sources. For studying weak matrix elements, we need a source of Goldstone pions at zero spatial momentum, uncontaminated by other light states, i.e., other pions. The $qq+oo$ source satisfies this requirement, since it produces only ρ's in addition to the Goldstone pion. A single source will always produce at least two pions, so we must use at least two sources. This still leaves many options, and our choice produces as many nonlocal states as possible, the Δ in particular. We note in passing that for the purposes of spectroscopy alone there exist even better sources which produce all possible states for the price of a single propagator calculation. For example, take the $\mathcal{A}(\eta)$ to be square roots of prime numbers, with a different prime for each corner η of the spatial cube. The disadvantage from our point of view is that it is then too expensive to project against the contamination from unwanted non-Goldstone pions.

To illustrate the filtering power of our sources, we show in Fig. 1(a) an effective mass plot for the correlator between the $qq+oo$ source and a qq sink, and in Fig. 1(b) a similar plot with the $qq-oo$ source (see Sec. VI for our definition of $m_{\rm eff}$). The results are for our lightest-quark mass on the $16^3\times 40$ lattices at $\beta=6$. The qq sink couples not only to the π, but also to the π_3, and to a number of ρ's as listed in Table I. The $qq+oo$ source should produce only the π and half of the ρ's, while the $qq-oo$ source should produce only the π_3 and the other one-half of the ρ's. The horizontal lines show the actual masses of the π and π_3. For this quark mass, the ρ's lie at

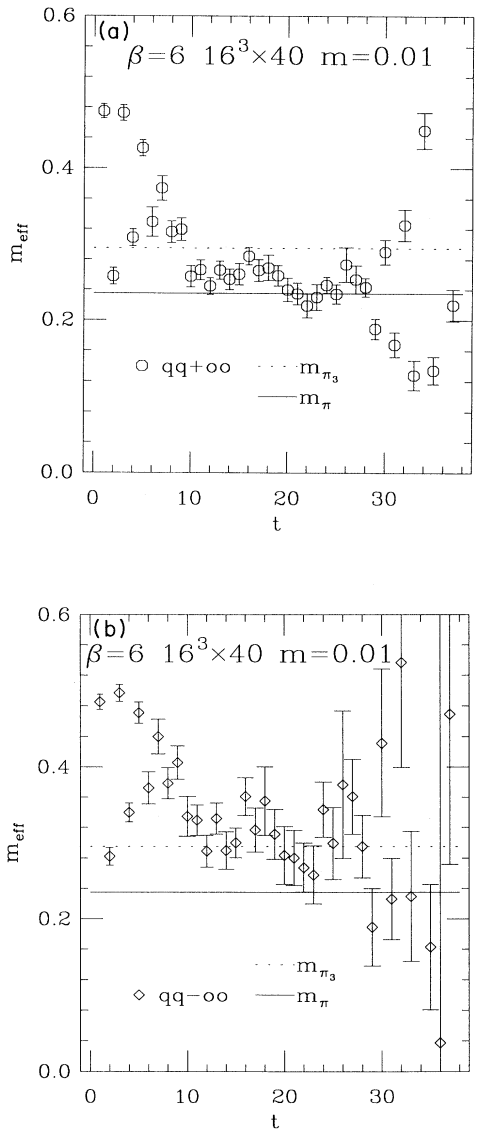

FIG. 1. Results for $m_{\rm eff}$ [Eq. (6.1)] for the $16^3\times 40$ lattices at $m_q=0.01$ at $\beta=6$. In both figures the source is fixed at $t=0$, while the sink moves from $t=0$ to 39. The sink is a qq extended operator, while the source is (a) $qq+oo$ and (b) $qq-oo$ in the two figures. The horizontal lines show the values of the π and π_3 masses.

$m_\rho \approx 0.45$. With the $qq+oo$ source we see that it takes 10 time slices for the Goldstone pion to become dominant, and that for $t>30$ there are large boundary effects due to our use of Dirichlet boundary conditions. The behavior for $t=10$–20 is slightly disturbing. The major effect is the undulation. This is present even if we use an extended operator which projects onto the π, and is not due to a contamination from the π_3. The small oscillation is due to a small contamination from the ρ's. The pattern is similar with the $qq-oo$ source, except that the errors are larger. The projection is more difficult here, since it must be done against the lighter π. There is some indication of a drop around $t=22$, but we have checked that this is not due to contamination with the π.

We end this section with a brief summary of alternative sources. One might expect that the major weakness of our source is that it is too large, since a source of typical hadronic size would be best for spectrum calculations. Such sources have been proposed by the APE Collaboration,[16] who use a cube source of typical hadronic size, and the Wuppertal group[18] who use a scalar propagator to smear the source on a time slice. The APE group has also suggested using a number of cubes or smeared sources of hadronic size spaced as far apart as possible—the multiorigin method.[19] Our conclusion, based on a comparison with the work of the APE group at $\beta=5.7$ (Ref. 20) is that for the lattice volumes used in this study, wall sources work comparably to cube sources.

It is possible, however, to include correlations in our zero-momentum wall sources. One method is to generate three-dimensional pseudofermions ϕ by solving $(-D_3^2+m_{\text{source}}^2)^{-1}\phi=\eta$, and then using ϕ as the source. Here η is a Gaussian noise vector on the source time slice, D_3 is the scalar covariant derivative restricted to the time slice, and m_{source} is a tunable mass parameter. Averaging over pseudofermions ensures zero spatial momentum, while correlations over a tunable distance are built in. The limit $m\to\infty$ corresponds to zero correlation, or a random gauge transformation at every site, just as in the original proposal of Ref. 14. The limit $m\to 0$ corresponds to long-range correlation, similar to a wall source. One might hope to find an optimum somewhere between the two extremes. We plan to test this idea in future work.

IV. OPERATORS

The wall sources produce a number of different states. To extract their masses, we would like to use operators which pick out only one representation. In fact, as discussed in Sec. II, the best that can be done is to couple to two representations, one oscillating, the other smooth. To do this we use two types of operators: extended and quasilocal. We will discuss these operators first for the mesons, and then the baryons.

For mesons, the extended operators are exactly those discussed in Sec. II, and are given explicitly in Eq. (2.4). The operators are made gauge invariant by requiring that the lattices are put into the Landau gauge. The advantage of these operators is that they form true representations of the zero spatial momentum time-slice group.[9] The main disadvantage is that, as mentioned previously, correlation functions of the Landau gauge operators do not have a transfer matrix interpretation. This is true despite the fact that one of the operators is in the Coulomb gauge, since the Landau gauge operator involves links everywhere on the lattice. A second disadvantage is that the correlators are noisier than those with quasilocal operators. In practice, the increased noise makes these correlators inferior to those with quasilocal operators. Nevertheless, in all channels with a signal the resulting masses are consistent with those from quasilocal operators.

The quasilocal operators are defined as follows. For the state $\Gamma_S\otimes\Gamma_F$, we use

$$\mathcal{O}'_{SF}(t)=\sum_{\mathbf{y}}\sum_{\eta,\eta'}\bar{\chi}[(2\mathbf{y},t)+\eta]\chi[(2\mathbf{y},t)+\eta'] \times \mathrm{Tr}(\Gamma_\eta^\dagger\Gamma_S\Gamma_{\eta'}\Gamma_F^\dagger)\ . \tag{4.1}$$

That is, in each hypercube we project onto the required spin and flavor and then sum over all 2^4 hypercubes whose origin lies in a given time slice. Most of the operators involve $\bar{\chi}$ and χ fields at different sites, and these are defined by using the Landau gauge. Thus these apparently quasilocal operators have some component spread out over all the lattice. We expect this to be much less of a problem than for the extended operators, since it is presumably suppressed by the small size of the "dipole." We can actually test this for the Goldstone pion because we can destroy the pion with the true axial-vector current, a manifestly gauge-invariant operator which couples only to physical states, and with a Landau gauge version of this operator in which the gauge link is absent. We find that, after a short transient period, the two correlators are proportional [with a ratio close to the value of $\mathrm{Tr}(U)/3$ given in Table II].

The other disadvantage of these operators is that they are not true representations of the time-slice group, except for those in which $S=F$ or $S=F+(0,0,0,1)$. One can write the operators as a sum of an operator which is a true representation, and a second operator which contains derivatives. The second operator will, in general, couple to states in other representations: ρ's will couple also to certain pion representations, and vice versa. One might expect this to be problematic for ρ's, since the pions are lighter. However, the second operator contains derivatives, and its overlap with the unwanted states is suppressed by the lattice spacing. In practice, we do not find such contamination to be a problem. Nevertheless, we recommend that future calculations avoid this problem altogether by using the somewhat more complicated quasilocal operators of Ref. 7, which are true representations of the time-slice group.

We use operators for all the spin flavors in Table I, together with the corresponding scalar and axial-vector channels obtained by $\Gamma_S\otimes\Gamma_F\to\gamma_4\gamma_5\Gamma_S\otimes\gamma_4\gamma_5\Gamma_F$. These are all LT operators, i.e., $\delta=S-F$ has no time component. We also use operators with an additional time link, i.e., $\gamma_4\Gamma_S\otimes\Gamma_F$ and $\gamma_5\Gamma_S\otimes\gamma_4\gamma_5\Gamma_F$. These NLT

TABLE II. Simulation parameters. The algorithms are pseudoheat bath (PHB), multihit Metropolis (Met) and an overrelaxed/Metropolis mixture (OR/Met) in the ratio of 4:1. The errors on $\langle \mathrm{Tr}(U) \rangle /3$ are less than 1 in the last digit. A dash indicates that the result is not available.

	β:	5.7	6.0	6.0	6.2
	Size:	$16^3 \times 32$	$16^3 \times 40$	$24^3 \times 40$	$18^3 \times 42$
Sample	(A)	12	21	15	32
	(B)	20	15	8	
Sweeps/config.	(A)	1000	300	500	250
	(B)	1000	1000	500	
Algorithm	(A)	OR/Met	OR/Met	OR/Met	Met
	(B)	PHB	PHB	OR/Met	
Landau iters		350	300	350	1000
Landau $\langle \mathrm{Tr}(U) \rangle /3$		0.824	-	0.8610	0.873
Coulomb iters		100	100	300	0
Coulomb $\langle \mathrm{Tr}(U) \rangle /3$		0.856	-	0.882	-
m_q		0.015, 0.01, 0.005	0.03, 0.02, 0.01	0.03, 0.02, 0.01	0.03, 0.02, 0.01, 0.007
Avg. CG iters		585, 628, 700	321, 361, 571	324, 361, 586	318, 437, 722, 1225

operators couple to the same states, but with different amplitudes. In fact, as explained in Ref. 2, the NLT operators reduce the contribution from oscillating states. This advantage is offset by the general tendency for the signal with NLT operators to die out faster. Which operator gives the best signal depends on the channel.

For baryons we use exactly the same two types of operators as for mesons, i.e., extended and quasilocal. The extended operators are made out of the extended quark fields following the construction given in Table 3 of Ref. 9, which we discussed previously in connection with wall sources. We construct operators of all possible classes, in all cases taking the same elements of the representations as are created by the wall source. Operators of classes 1 and 5 couple only to the **8** (class 1 is the familiar local baryon), while class 7 operators couple only to the **8′**. Our operators of classes 3 and 6 couple to both the **8** and **16**, while our class 4 operators to both the **8′** and **16**. Thus we only expect a pure Δ signal with the class 7 operator. This operator has the quarks all separated from each other by two links, e.g., one quark at $\hat{\mathbf{x}}$, the second at $\hat{\mathbf{y}}$ and the third at $\hat{\mathbf{z}}$. All other operators couple to the nucleon, but have different coupling to the excited states. In fact we find, at $\beta=6$ and 6.2, that some class 4 and 6 operators show a Δ signal at small times and a nucleon signal at long times.

We can improve the quality of the signal using quasilocal operators which, as for the mesons, are not true representations of the lattice time-slice symmetry group. In these, the three quark fields are contained in the same spatial 2^3 cube, and then one sums over the cubes in the time slice. The class of the operator is determined by the relative positions of the quarks in the cube just as for the extended operators. Again we form operators of all classes, but now the class 7 operator not only couples to the Δ but can also couple to the nucleon by terms suppressed by the lattice spacing.

We have also used NLT operators in which one of the three quarks is translated in the time direction, but with all other phases unchanged. This does not change the representations that are created, but it does reduce the amplitude of the oscillating opposite-parity component. We use such NLT variants of both extended and quasilocal operators. As for the mesons, the disadvantage of the NLT channels is that the signal tends to last for less time. For the Δ, however, the signal only extends to relatively short times, and the NLT operator is preferred. Since we want to be sure that we are seeing the Δ, we try to use the NLT variant of the extended class 7 operator, which we call the "true" Δ operator. Unfortunately, the signal is only good enough at $\beta=6.2$. For $\beta=6$, we are forced to use the NLT quasilocal class 7 operator.

Clearly it would be better to use the quasilocal operators of Ref. 7 which truly represent the time-slice group. Our experience suggests that NLT variants of these operators would be the best choice.

V. CALCULATION DETAILS

The lattices have been generated using a variety of algorithms: multihit Metropolis, Cabibbo-Marinari pseudoheat bath, and a combined overrelaxed/Metropolis method. All configurations have been generated using periodic boundary conditions in space and time. More details can be found in Ref. 21. We list in Table II the important statistics of the various ensembles that we use. We have chosen the number of sweeps between analyzed configurations to produce an essentially decorrelated sample of lattices.

As mentioned above, we use a hybrid gauge for our propagator calculations. The gauge fixing is done in two steps. First we transform the lattice to the Landau gauge using an overrelaxed algorithm described in Ref. 22. The boundary conditions remain periodic in space and time. Next, we fix the source time slices to the Coulomb gauge. Table II also gives the parameters of these two gauge-fixing steps.

In all calculations of propagators we use periodic boundary conditions (PBC's) in space and Dirichlet boundary conditions (DBC's) in time. We calculate prop-

agators using two positions for the wall source. For the lattices at $\beta=5.7$ and 6.0, we place the wall sources on the first and last time slices, i.e., the time slices adjacent to the boundary. On the $\beta=6.2$ lattices we place the sources at $t=3$ and 38, using the convention (as is done throughout this paper) that the lattice time ranges from $t=0$ to $t=(N_t-1)$. We use DBC in time primarily because it simplifies our calculation of weak matrix elements. It has been argued, however, that DBC are inferior to (A)PBC for spectrum calculations, because of reflections from the boundary.[23] We find that, on the contrary, the fact that the signal extends in many channels across the entire lattices makes DBC preferable.

The quark propagators are calculated using a standard conjugate-gradient algorithm, in which we solve only for the even half of the points, and construct the odd half at the end. We have made the following improvements compared to our previous work.[2]

(1) We rotate to temporal gauge during the calculation, which removes one quarter of the multiples by gauge matrices. At the end of the computation we rotate the propagator back to the hybrid gauge.

(2) To reduce memory charges we pack the 18 real numbers of the gauge links into five 64-bit words. We have checked that the small changes in the gauge links that are introduced by this packing have an effect on the masses which is much smaller than the statistical errors.

(3) The code is multitasked, which again reduces memory charges. The various tasks calculate the action of $\not{D}$ on different parts of the vector. The typical overlap, on a four processor Cray 2, is ~ 2.

On each configuration we calculate four propagators at each quark mass: q and o sources at both ends of the lattice. The quark masses that we use are given in Table II. In all cases we run propagators until the residual satisfies

$$|r_e|^2=|(\not{D}^2-m^2)G_e+mS_e-\not{D}S_o|^2\leq 10^{-11}|G_e|^2 , \quad (5.1)$$

where G is the propagator, S is the source, and the subscripts refer to even and odd parts. Our tests indicate that this is a conservative choice. To illustrate this claim, we show in Fig. 2 how one of the ρ propagators at $t=25$ varies as a function of our convergence parameter $(r_e/G_e)^2$. The answer reaches a stable value at roughly 10^{-10}, though it is not converged at all before 10^{-9}. The signal in this channel does not extend to $t=25$, so the quantity plotted is in the statistical noise. The figure shows that this noise, which hides the ρ signal, is due to the finite size of our sample of configurations, and does not come from a lack of convergence of the propagators. For our weak matrix element calculations, it is important that we know the converged value of correlators in channels such as that shown.

Table II lists the number of iterations that are required to reach an accuracy of 10^{-11}. The only exceptions are for $m=0.005$ at $\beta=5.7$, and for all inversions at $\beta=6.2$, for which the criterion was relaxed to $|r_e|^2\leq 10^{-10}|G_e|^2$. For all but the highest masses, we use a starting seed, obtained by polynomial extrapolation from the propagators at higher masses. This simple expedient saves roughly 290 iterations at $\beta=6.0$, or about 20% overall.

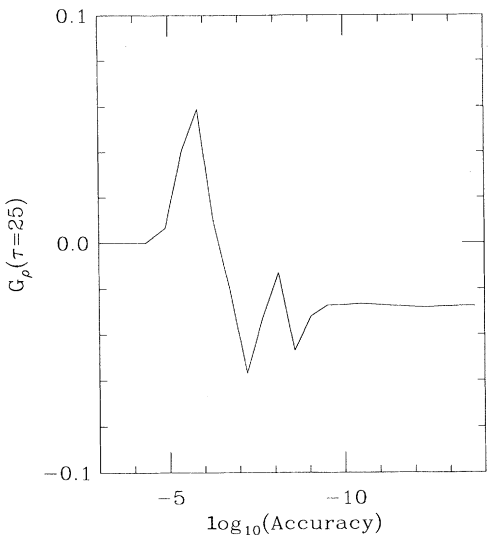

FIG. 2. A ρ correlator on one configuration at $m=0.03$ and $t=25$ as a function of convergence on the $16^3\times 40$ lattice at $\beta=6.0$.

VI. EXTRACTING MASSES

The extraction of reliable mass estimates from the hadron correlators is a potential source of systematic errors. In our previous work we fit the correlators to a sum of two exponentials over a certain range of times. For correlators other than that of the Goldstone pion, one of the exponentials oscillates in time, corresponding to the opposite-parity partner. By varying the fitting range we obtained some estimate of the reliability of the results. We then confirmed this by looking at the plots of the correlator. Errors were estimated using the jackknife or bootstrap methods, though using only the diagonal part of the error matrix to do the fitting.

We now think that, except for channels with clear signals (namely, the pions and some of the ρ's), we substantially underestimated the errors due to fitting. The problem was partly caused by not using the full error matrix, so that we did not know the goodness of fit. More important, however, was the fact that we assessed the reliability of the fits by looking only at log plots of the correlators. In a number of cases we ended up fitting to regions where the data was unreliable, or had clearly not reached the region of asymptotic fall-off.

We improve on this method here by (a) using the full error matrix, so that we know when our time range is too large because the goodness of fit deteriorates, and (b) using plots of the effective mass (rather than the correlator itself) to see whether the mass has reached its asymptotic value. For staggered fermions, the transfer matrix is defined for two time steps, so we use

$$m_{\rm eff}(t)=\tfrac{1}{2}\ln\left[\frac{C(t)}{C(t+2)}\right] , \quad (6.1)$$

where C is a hadron correlator. We use the jackknife

TABLE III. Meson spectrum for staggered fermions at $\beta=5.7$ on a $16^3\times 32$ lattice.

	π		π_3		ρ_6^A	
m_q \ fit	8–18	χ^2/N_{DF}	2–8	χ^2/N_{DF}	2–7	χ^2/N_{DF}
0.015	0.350(1)	6/7	0.71(2)	2/3	0.93(3)	0.4/2
0.015+0.010	0.322(1)	5/7	0.69(2)	1/3	0.91(4)	0.3/2
0.01	0.289(1)	4/7	0.67(2)	1/3	0.89(4)	0.2/2
0.015+0.005	0.289(1)	5/7	0.66(2)	1/3	0.89(4)	0.2/2
0.010+0.005	0.252(1)	6/7	0.64(2)	1/3	0.86(5)	0.1/2
0.005	0.208(1)	8/7	0.61(3)	1/3	0.82(7)	0.1/2

method to calculate the errors in $m_{\rm eff}$. In a typical channel (see, for example, Figs. 4 and 5) the effective mass grows, then reaches a plateau, and then becomes noise. As will be discussed further in Sec. VIII, it is possible for the fitting program to give a reasonable fit for a small set of time ranges (particularly if one does not use the full error matrix), and yet for it to be apparent from the plot of $m_{\rm eff}$ that the asymptotic plateau has not been reached.

Note that the approach to the asymptotic value need not be from above because our correlators are not diagonal: we use extended operators to create the states out of a Dirichlet boundary condition, and quasilocal operators to destroy them into something more like the usual vacuum. Thus contributions to the correlators are not positive definite.

Our fitting method consists of first determining from the effective mass plot whether there is a plateau region. If so we use the above-mentioned fit to two exponentials in that region. We calculate the full error matrix using the entire sample, and then estimate errors using single elimination jackknife, fitting for each subsample using the full error matrix. We estimate the goodness of fit using the average χ^2 of the fits for each of the subsamples. Typically we quote results from the largest time range available, and estimate a systematic error due to fitting by varying the time range. With much of our data we find this error to be at least as large as the statistical error, and sometimes 2–3 times larger. This is due to undulations in the plateaus.

We try to avoid the spurious fits of our previous work by not quoting a value if there is not a clear plateau. Of course, the choice of what constitutes clarity in a plateau is somewhat subjective. We try to make clear in the text which of the results we quote have large uncertainties. For example, we have not found reliable signals for any of the positive-parity mesons (a_0,a_1, and b_1) or negative-parity baryons.

VII. $16^3\times 32$ LATTICES AT $\beta=5.7$

We begin with results from a relatively strong coupling, $\beta=5.7$. Calculating at this coupling allows us to use a large lattice in physical units, and thus work at small physical pion masses. We use quark masses 0.005, 0.010, and 0.015, corresponding to pion masses ranging from roughly 200 to 400 MeV. Having such light masses is important for our study of weak matrix elements, since it allows us to examine their chiral behavior. Unfortunately, the signals for states other than the Goldstone pion are poor. Thus, the major functions of the calculation are to indicate how rapidly quantities vary with β, and to cross-check the results of the APE Collaboration.[20]

Our result for the mesons are given in Table III, and for the nucleon (we have no signal for the Δ) in Table IV. Figures 3(a)–3(c) show examples of the signals on which these results are based. For the mesons we quote results for the largest time range falling within the plateau for all quark masses. All fits are reasonable, having $\chi^2/N_{DF}\leq 1$. For the nucleon, there is no plateau, so we quote $m_{\rm eff}$ at the largest two times with reasonable errors ($t=3$ and 4). The quoted errors are purely statistical; we discuss systematic effects in the following.

The Goldstone-pion signal is of good quality. We use the NLT operator $\gamma_4\gamma_5\otimes\gamma_5$, since it has a plateau in $m_{\rm eff}$ which begins earlier than that for the LT operator $\gamma_5\otimes\gamma_5$. As Fig. 3 shows, the plateau for the NLT operator begins almost at $t=1$, and extends to $t=20$–24 (the precise value depending on m_q), at which time boundary effects become important. We quote numbers using the range $t=8$–18. At all except the lightest-quark mass, fitting to other reasonable time ranges, or using the LT operator, gives numbers consistent with those quoted to within $\sim 1\sigma$. At the lightest mass, the LT operator gives $m_\pi=0.205(1)$, which is 3σ below the NLT value. Thus the systematic errors coming from the fitting are somewhat larger than the statistical errors.

Our result for the Goldstone pion agree well with the behavior $m_\pi^2\propto m_q$ expected in the chiral limit. Fitting to $m_\pi^2=A_\pi m_q+B_\pi$ we find $A_\pi=7.96(5)$ and $B_\pi=0.004(1)$. The slight deviation of B_π from zero may

TABLE IV. Values for $m_{\rm eff}$ for the nucleon at $\beta=5.7$ on a $16^3\times 32$ lattice.

m_q	$m_{\rm eff}(t=3)$	$m_{\rm eff}(t=4)$
0.015+0.015+0.015	1.22(3)	1.14(7)
0.010+0.015+0.015	1.20(3)	1.12(8)
0.010+0.010+0.015	1.18(3)	1.09(9)
0.010+0.010+0.010	1.15(4)	1.07(10)
0.005+0.010+0.010	1.13(5)	1.06(13)
0.005+0.005+0.010	1.12(6)	1.06(18)
0.005+0.005+0.005	1.11(9)	1.09(26)

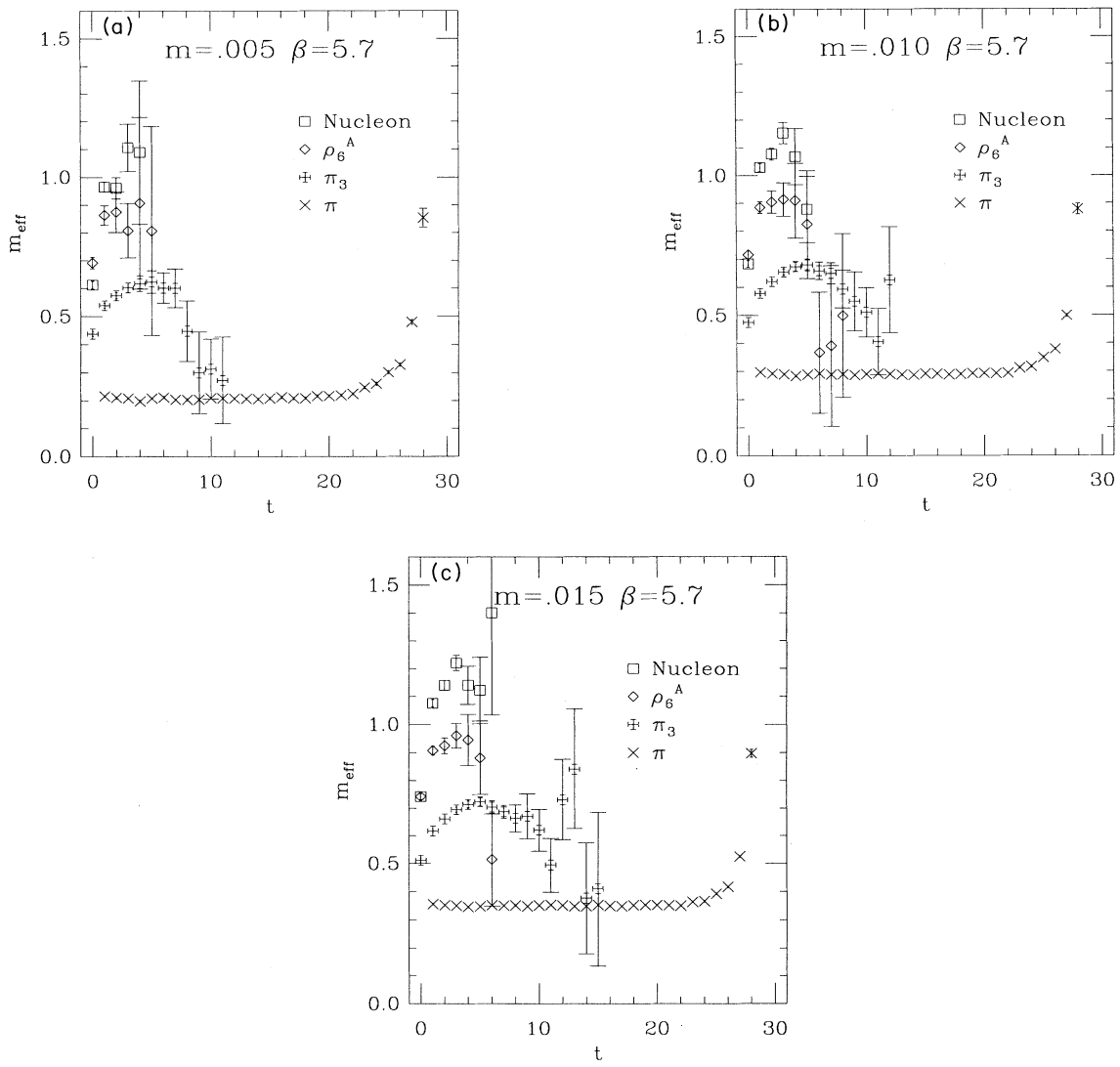

FIG. 3. Effective mass plot for the π, π_3, ρ_6^A, and nucleon on the $16^3\times 32$ lattices at $\beta=5.7$ for (a) $m_q=0.005$, (b) $m_q=0.010$, and (c) $m_q=0.015$. The lattice runs from $t=0$ to 31, with the wall source at $t=0$.

be an indication of finite-size effects at the lightest-quark masses.

The best signal from the non-Goldstone pions is for the π_3, using the LT operator. As Fig. 3 shows, the signal degenerates into noise by $t=8$ for the lightest-quark mass, and by $t=10$ for the heaviest. One can still extract a mass with some reliability, although the errors are clearly quite large. The signals for the $\bar{\pi}$ and $\bar{\pi}_3$ are poorer, but the effective mass plots show that all three non-Goldstone pions are degenerate within large ($\sim 10\%$) errors. All three are thus much heavier than the Goldstone pion, so that flavor symmetry is badly broken, as we would expect at such strong coupling.

The signal deteriorates further when we look at the ρ's. Table III and Fig. 3 only give results for the operator $\gamma_3\otimes\gamma_2$, which creates a ρ_6^A state. All other ρ channels have comparable or worse signals, and all lead to consistent estimates of m_ρ. Our results are not good enough to demonstrate the existence of a plateau in $m_{\rm eff}$; the possible plateau beginning at $t=1$–2 disappears into noise by $t=5$–6. To quote a mass we fit to the range $t=2$–7 (corresponding to $t=2$–5 in the $m_{\rm eff}$ plot). Clearly these estimates are subject to significant systematic errors.

Finally, we turn to the nucleon. We quote results for the operator with the cleanest signal, which turns out to be a LT operator in class 2 of Ref. 9. It consists of a sum of terms with two quarks on one site, and the other separated by a link in the z direction. At the highest-quark mass, there is evidence for a plateau from $t=2$–5, but at the lowest-quark mass there is no plateau. Because of this, we simply quote in Table IV the values of $m_{\rm eff}$ at $t=3$ and 4.

At $m_q=0.01$, we can directly compare our results with those of the APE Collaboration.[20] They use three different sized lattices, and have samples of similar size to ours: 60 of size $12^3\times24$, 20 of size $18^3\times24$, and 50 of size $24^3\times32$. They use a smaller source—a "cube" (three lattice units on a side) rather than a "wall." Also, the phase, $\mathcal{A}(\eta)$ in Eq. (3.1), is zero except at $\eta=0$, so that the source only creates local states. Thus we can only directly compare the π and nucleon masses (they do not quote a result for the $\tilde{\pi}$). It is, however, reasonable to compare the results for m_ρ, since we find all ρ's to be degenerate within errors.

Our result for the pion mass at $m_q=0.01$ [$m_\pi=0.289(1)$] agrees within $\sim1.5\sigma$ with both their 24^3 lattice value [0.2876(7)] and their 18^3 result [0.283(3)]. In the ρ channels the APE group finds a clear plateau in $m_{\rm eff}$ only on their largest lattice, the plateau consisting of four points, and yielding $m_\rho=0.88(6)$. Our results at $m_q=0.01$ [Fig. 3(b)] are very similar, in terms both of the number of useful points and of the resulting value of m_ρ[0.89(4)]. This implies that our wall source has an efficacy similar to the cube source used by APE.

The comparison of the nucleon mass is less satisfactory. The APE results are reliable only on the 24^3 lattice, and they find $m_N=1.454(26)$. This is many standard deviations above all our points in Fig. 3(b). We can also compare at $m_q=0.015$, for which our data is better, with evidence for a plateau at $m_N\approx1.15$. The average of the APE results for $m_q=0.01$ and $m_q=0.02$ is $m_N=1.48(2)$, again much above our data. The APE results are not given in the form of an effective mass plot, so we cannot directly compare the quality of our data with theirs. We suspect that neither group has found the asymptotic result for m_N.

VIII. $16^3\times40$ AND $24^3\times40$ LATTICES AT $\beta=6$

Our most extensive data is at $\beta=6$, for which we have both "small" ($16^3\times40$) and "large" ($24^3\times40$) lattices. This allows us to search for finite-volume effects, both in the masses themselves, and in the performance of the wall sources. The quark masses used are heavier than for $\beta=5.7$: $m_q=0.01$, 0.02, and 0.03, which correspond approximately to $m_s/2$, m_s and $3m_s/2$. We use two independent samples of lattices for both sizes (see Table II) and we find no significant differences in hadron masses between the samples. For the small lattices we quote results for the combined data sample. For the large lattices, however, the source time slice for the smaller sample was inadvertently fixed to the Landau rather than the Coulomb gauge, so we cannot simply combine it with the larger sample. Thus we quote results only from the larger sample of 15 lattices.

We collect our results for hadron masses in Tables V and VI, and show in Fig. 4 the correlators at the lightest and heaviest quark masses. The errors are purely statistical, and the goodness of fit can be gauged by the $\chi^2/N_{\rm DF}$. The results for $m_q=0.01+0.03$ are not shown since they are essentially identical to those for $m_q=0.02$. In preparing these tables we have to choose the time range for the fits, and select between various operators. We have studied the dependence of the masses on these choices in order to estimate the systematic errors due to fitting. We now discuss these points in some detail for each state.

The best estimate of the Goldstone-pion mass comes from the LT operator. The difference between the LT and NLT operators is shown in Fig. 5 for the lightest-quark mass. The NLT channel has a plateau which begins slightly earlier (as discussed above), but this is more than compensated by the earlier onset of boundary effects. At heavier-quark masses the plateau is longer, so a fitting range suitable for all masses is $t=12$–28. Unfortunately, we have too few large lattices to invert the correlation matrix for such a long-time range, so we fit to $t=15$–25 and to $t=12$–21 on both lattice sizes. Comparing these two time ranges we see variations in m_π on a given lattice size of up to 3σ. This is caused by the plateaus not being flat. In Fig. 5, for example, the LT pla-

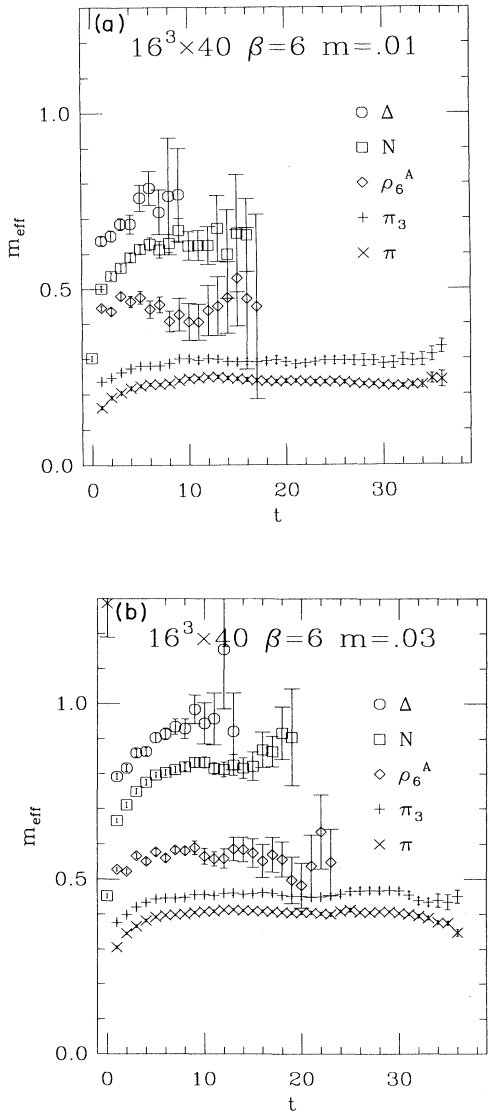

FIG. 4. Effective mass plots for the π (LT operator), π_3 (LT), ρ_6^A (LT), nucleon (NLT) and Δ (NLT) at $\beta=6$ on $16^3\times40$ lattices. (a) $m_q=0.01$ (b) $m_q=0.03$.

TABLE V. (a) The pion spectrum at $\beta=6$ on both size lattices. We quote the masses, χ^2 (using correlated errors), and the number of degrees of freedom ($N_{\rm DF}$). The results of two fits on each lattice are shown. (b). The ρ spectrum at $\beta=6$ from the two lattices. The notation is as in (a).

(a)

Staggered pion spectrum at $\beta=6$

m_q	Fit	π	π_3	$\tilde{\pi}_3$	$\tilde{\pi}$
0.03+0.03	15–25(24^3)	0.417(2)	0.461(2)	0.474(5)	0.451(4)
	$\chi^2/N_{\rm DF}$	8/7	10/7	14/7	19/7
	15–25(16^3)	0.407(2)	0.451(6)	0.461(3)	0.449(3)
	$\chi^2/N_{\rm DF}$	3/7	6/7	4/7	9/7
	12–21(24^3)	0.412(2)	0.461(3)	0.461(3)	0.463(4)
	$\chi^2/N_{\rm DF}$	15/6	15/6	40/6	17/6
	12–21(16^3)	0.410(3)	0.457(3)	0.469(5)	0.456(4)
	$\chi^2/N_{\rm DF}$	6/6	9/6	7/6	8/6
0.03+0.02	15–25(24^3)	0.382(2)	0.426(3)	0.439(5)	0.417(4)
	$\chi^2/N_{\rm DF}$	9/7	13/7	12/7	16/7
	15–25(16^3)	0.373(2)	0.424(3)	0.424(3)	0.414(3)
	$\chi^2/N_{\rm DF}$	3/7	7/7	6/7	7/7
	12–21(24^3)	0.376(2)	0.425(3)	0.428(2)	0.429(4)
	$\chi^2/N_{\rm DF}$	15/6	13/6	32/6	20/6
	12–21(16^3)	0.375(3)	0.422(4)	0.436(5)	0.422(4)
	$\chi^2/N_{\rm DF}$	7/6	11/6	6/6	7/6
0.02+0.02	15–25(24^3)	0.342(2)	0.386(3)	0.399(3)	0.381(3)
	$\chi^2/N_{\rm DF}$	10/7	18/7	13/7	11/7
	15–25(16^3)	0.334(2)	0.383(7)	0.387(3)	0.379(3)
	$\chi^2/N_{\rm DF}$	3/7	6/7	10/7	6/7
	12–21(24^3)	0.336(2)	0.386(3)	0.393(3)	0.392(4)
	$\chi^2/N_{\rm DF}$	15/6	11/6	29/6	21/6
	12–21(16^3)	0.337(3)	0.384(4)	0.401(5)	0.386(4)
	$\chi^2/N_{\rm DF}$	7/6	10/6	5/6	5/6
0.01+0.02	15–25(24^3)	0.296(2)	0.342(6)	0.353(2)	0.345(4)
	$\chi^2/N_{\rm DF}$	12/7	30/7	147/7	13/7
	15–25(16^3)	0.286(15)	0.340(3)	0.343(5)	0.342(6)
	$\chi^2/N_{\rm DF}$	5/7	5/7	13/7	4/7

teau slopes slightly downwards, while the NLT plateau slopes more prominently upwards. We also find up to 3σ variations in m_π between LT and NLT operators. All this indicates that the systematic errors due to fitting are considerably larger than the quoted errors. The real errors are ~2–3 %, rather than the 0.5–1 % statistical errors.

For all the non-Goldstone pions we can use the same fitting ranges as for π. The signal for the π_3 is illustrated in Fig. 4. For the π_3 the LT channel gives the best signal, while for the $\tilde{\pi}_3$ and $\tilde{\pi}$, the NLT operators are better. Some of the fits to these channels are very poor, particularly for the $\tilde{\pi}_3$ at small quark mass. This is due to undulations in the plateau, the worst example of which (corresponding to the terrible fit with $\chi^2/N_{\rm DF}=147/7$) is shown in Fig. 6. Once again the systematic errors are a few times the statistical errors.

We give results for only one of the ρ channels, the ρ_6^A created by the LT operator $\gamma_3\otimes\gamma_2$. We examine all 12 channels (belonging to eight different representations as explained in Sec. II), and find the others to be of similar

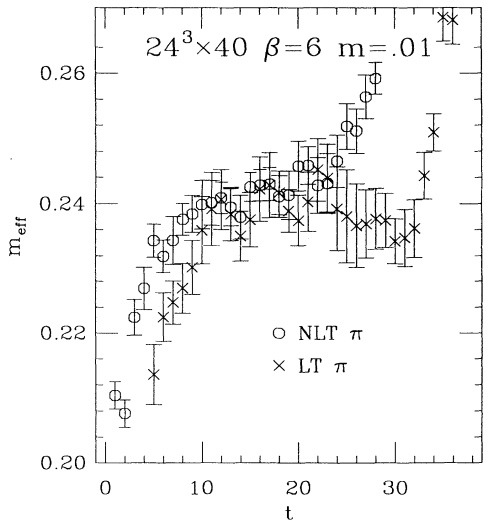

FIG. 5. Effective masses for the Goldstone pion on $24^3\times40$ lattices at $\beta=6$ using the LT and NLT operators.

TABLE V. (*Continued*).

(a)

Staggered pion spectrum at $\beta=6$

m_q	Fit	π	π_3	$\tilde{\pi}_3$	$\tilde{\pi}$
	12–21(24^3)	0.291(2)	0.342(3)	0.349(3)	0.349(2)
	$\chi^2/N_{\rm DF}$	13/6	9/6	26/6	10/6
	12–21(16^3)	0.293(3)	0.341(4)	0.363(5)	0.348(4)
	$\chi^2/N_{\rm DF}$	10/6	7/6	7/6	3/6
0.01+0.01	15–25(24^3)	0.239(1)	0.295(2)	0.314(6)	0.295(3)
	$\chi^2/N_{\rm DF}$	19/7	38/7	54/7	22/7
	15–25(16^3)	0.234(10)	0.291(5)	0.296(7)	0.297(6)
	$\chi^2/N_{\rm DF}$	6/7	3/7	15/7	7/7
	12–21(24^3)	0.237(2)	0.288(2)	0.319(6)	0.300(3)
	$\chi^2/N_{\rm DF}$	14/6	12/6	31/6	6/6
	12–21(16^3)	0.242(3)	0.295(4)	0.322(7)	0.301(4)
	$\chi^2/N_{\rm DF}$	7/6	3/6	10/6	4/6

(b)

Staggered ρ spectrum at $\beta=6$

m_q	Fit	ρ_6^A	$\chi^2/N_{\rm DF}$
0.03+0.03	6–16(24^3)	0.562(4)	11/7
	6–16(16^3)	0.575(7)	3/7
0.03+0.02	6–16(24^3)	0.537(5)	10/7
	6–16(16^3)	0.546(9)	2/7
0.02+0.02	6–16(24^3)	0.51(1)	12/7
	6–16(16^3)	0.52(1)	1/7
0.01+0.02	6–16(24^3)	0.49(1)	13/7
	6–16(16^3)	0.48(1)	1/7
0.01+0.01	6–16(24^3)	0.45(2)	16/7
	6–16(16^3)	0.44(2)	4/7

or slightly worse quality, and that all give consistent values of m_ρ. The ρ has a respectable plateau, particularly at the heavier mass, and we fit to $t=6$–16 (corresponding to 6–14 on the $m_{\rm eff}$ plots.) There is not much freedom to vary the range of the fit, but, to the extent we can, the central value for m_ρ does not change by more than 1σ.

For the nucleon, we have to choose from a number of channels involving different spatial separations of the quarks, as well as between LT and NLT operators. It turns out that there is little difference between the various spatial separations, so we use the spatially local operator since this allows direct comparison with previous work. The plateau is slightly shorter than for the ρ, mainly because it begins at a later time, and we fit to $t=10$–18. Rather than choose between LT and NLT channels, we quote results for both in Table VI. The

TABLE VI. Nucleon spectrum at $\beta=6$ on both size lattices and using both LT and NLT operators. All fits are to $t=10-18$, so there are five degrees of freedom.

Type \ (size)	LT(16^3)		NLT(16^3)		LT(24^3)		NLT(24^3)	
m_q	m_N	χ^2	m_N	χ^2	m_N	χ^2	m_N	χ^2
0.03+0.03+0.03	0.84(1)	6	0.84(4)	4	0.83(1)	10	0.84(4)	4
0.02+0.03+0.03	0.82(1)	4	0.79(2)	3	0.79(2)	10	0.80(1)	4
0.02+0.02+0.03	0.79(1)	3	0.76(2)	5	0.75(3)	9	0.78(2)	4
0.02+0.02+0.02	0.77(2)	2	0.72(5)	4	0.72(3)	9	0.75(3)	3
0.01+0.02+0.02	0.74(2)	1	0.69(2)	3	0.67(2)	7	0.71(4)	3
0.01+0.01+0.02	0.71(2)	1	0.67(4)	2	0.64(1)	3	0.67(4)	3
0.01+0.01+0.01	0.69(3)	1	0.63(4)	1	0.61(2)	2	0.61(5)	5

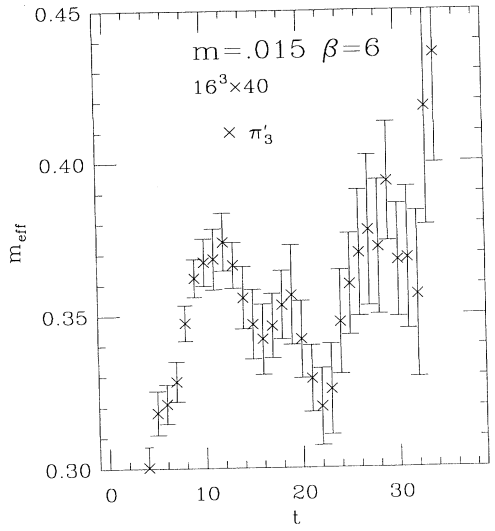

FIG. 6. Effective mass for the $\tilde{\pi}_3$ for $m_q=0.015$ (0.01+0.02) on the $24^3\times 40$ lattices at $\beta=6$.

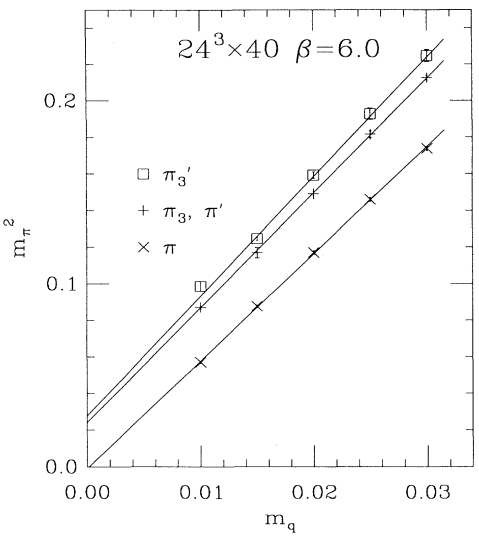

FIG. 7. The chiral behavior of m_π^2 from the $24^3\times 40$ lattices at $\beta=6$. The lines show linear fits.

differences between the channels can be seen by comparing Figs. 9(a) and 9(b), and we will discuss them in detail below.

Figures 4(a) and 4(b) also show a signal for the Δ. This uses the quasilocal NLT operator (in class 7 of Ref. 9), which, as discussed in Sec. III, is not a pure Δ operator, since it can couple to the nucleon through terms suppressed by the lattice spacing. The signal lies significantly above that for the nucleon, however, and we take this as evidence that a heavier Δ exists, though we do not quote masses. Fortunately, the evidence is more convincing at $\beta=6.2$. Several other mixed channels (e.g., in class 4 operators which couple to both the $\mathbf{8}'$ and the $\mathbf{16}$) show a "Delta" signal at early times and then drop to a nucleon plateau.

There are several marked differences compared to results at $\beta=5.7$. This can be seen most clearly by comparing Figs. 3 and 4. For a start, the data for the non-Goldstone pions, ρ's and baryons is much cleaner. This is consistent with previous experience that signals improve rapidly just beyond the "crossover" region in which the nonperturbative β function has a dip. Second, the staggered flavor symmetry is much less strongly broken in the pion sector than at $\beta=5.7$, confirming earlier results.[12,23] In addition, at $\beta=6$, all 12 ρ's that we measure are degenerate, within the 2–5 % errors. This is a weak bound, however, because we see no closer degeneracy between those ρ's which lie in the same lattice representation (and thus should be degenerate even at finite lattice spacing) than between ρ's in different representations.

For pions there is the usual gap between Goldstone and non-Goldstone pions. This is shown in Fig. 7, where we plot the values for m_π^2 on the large lattice [using the fit from Table 5(a) with the greater confidence level]. The π_3 and $\tilde{\pi}$ are nearly degenerate, while there are indications that $\tilde{\pi}_3$ is slightly heavier. Figure 7 also shows fits of m_π^2 to $A_\pi m_q + B_\pi$. As usual, the Goldstone pion extrapolates to the origin with good accuracy, as required by the chiral symmetry of staggered fermions.[8] The parameters of the fit for the Goldstone pion are $A_\pi=5.87(6)$ and $B_\pi=-0.001(1)$.

An important issue is whether the hadron masses depend on the volume. For the Goldstone pions, Table V(a) does show a systematically higher value from the larger lattice at the heavier values of m_q. The difference, however, is of the same size as the uncertainty due to varying the fitting range. The situation is clarified by looking directly at the corresponding effective mass plots, which are shown for the heaviest-quark mass in Fig. 8. It is the lack of a flat plateau in the results from the small lattice

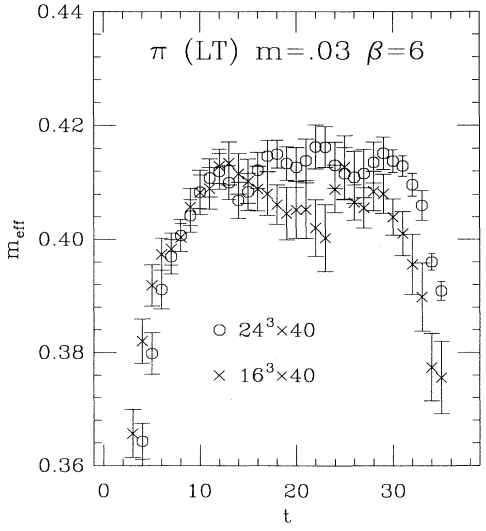

FIG. 8. Finite-volume effects in the effective mass of the π using the LT operator. Results are for $m_q=0.03$ at $\beta=6$.

which are the cause of the fitting uncertainty. We cannot conclude that there is a real finite-size effect until we see a clear difference between two flat plateaus. What we can conclude is that finite-size effects are small, at the level of 2% or less.

For the non-Goldstone pions and the ρ's there is no volume dependence within the errors, which are somewhat larger than those for the Goldstone pion. The correlators agree well at all times: the plateaus in $m_{\rm eff}$ begin at the same time, and the transients are very similar. In fact, the same is true for the Goldstone pion for $t \leq 15$ in Fig. 8.

For the nucleon, Table VI shows no volume dependence at the larger quark masses, but a confusing pattern of variations at the lightest-quark mass. In particular, there is, for $m_q=0.01$, a 2–3σ difference in m_N between lattice sizes if one uses LT operators, but no significant difference if one uses NLT operators. On the large lattice the two types of operators give consistent masses while on the small lattice the mass from the LT operator is higher. Clearly the statistical and systematic errors prevent us from making definite statements. It is important to note, however, that the bounds on finite-volume effects coming from our results are weaker than for the pion. The effect could be as large as 10% at the smallest quark mass.

There is, however, a clear finite-volume dependence in the transients. This is illustrated in Fig. 9 for the lightest-quark mass, but the same features are apparent for all quark masses. With LT operators there exists both an opposite-parity contribution (giving the oscillations) and an excitation of the same parity but opposite amplitude (giving the initial rise). For the NLT operators, the opposite-parity contribution is absent. For both operators the same finite-volume effect is apparent: the transients persist for longer time on the larger lattice. This is as expected, since the difference between the wall sources operators on the large and small lattices is a sum of operators with the quark and antiquark at large separation. These operators increase the coupling of excited states relative to the ground state.

Another issue we can comment on is the volume dependence of statistical errors. We find that the errors from 15 large lattices are somewhat smaller than those from 36 small lattices. This is consistent with the hypothesis that the extra volume of the large lattices gives independent information. If so, one would expect the errors to be smaller by a factor of $\sqrt{(15/36)\times(24/16)^3} \approx 1.2$, roughly consistent with what we find.

Finally we compare results with earlier calculations. Both Refs. 24 and 23 have results at the lighest-quark mass $m_q=0.01$. The former work uses five $16^3\times 32$ lattices, with three point sources on each configuration, the latter a single source on each of the 32 $16^3\times 24$ lattices. Thus we can only directly compare local states, i.e., the $\pi,\tilde{\pi}$, and the nucleon. Reference 24 quotes $m_\pi=0.249(4)$ and $m_N=0.728(95)$, whereas Ref. 23 has $m_\pi=0.247(3)$ and $m_{\tilde{\pi}}=0.312(47)$ (they use APBC in space which makes extracting the nucleon mass difficult). These are to be compared to our results on $16^3\times 40$ lattices: $m_\pi=0.242(3)$ [or $m_\pi=0.234(10)$, see Table V(a)],

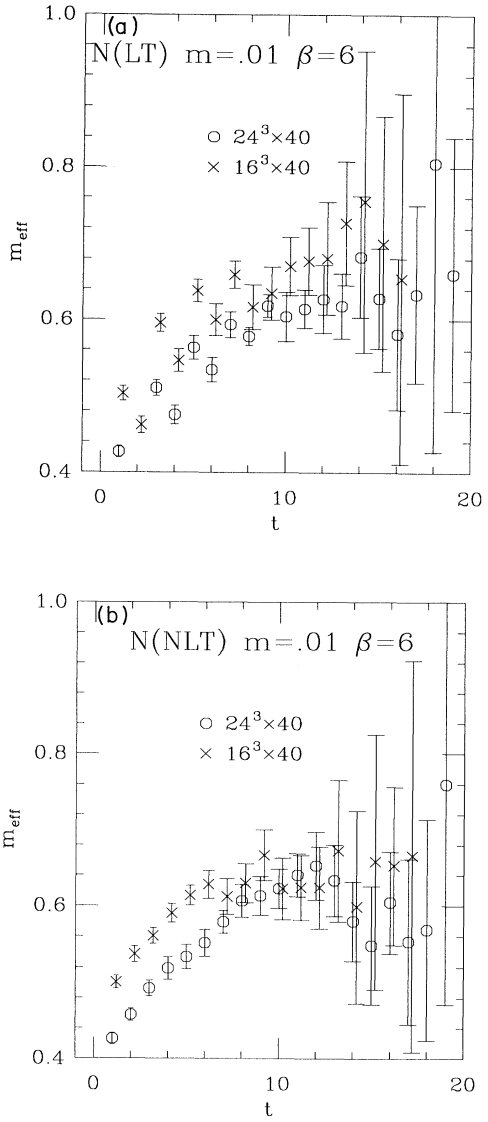

FIG. 9. Finite-volume effects in the effective mass of the nucleon using (a) LT and (b) NLT operators. Results are for $m_q=0.01$ at $\beta=6$. A slight horizontal offset has been added to the $16^3\times 40$ results.

$m_{\tilde{\pi}}=0.297(6)$ and $m_N=0.69(3)$ (using the LT operator as used in Ref. 24). The agreement is reasonable. For the ρ's, Ref. 24 quote $m_\rho=0.50(5)$ and 0.39(6) for the two local ρ's, while Ref. 23 find $m_\rho=0.62(7)$ and 0.66(18) from poor fits. These are clearly consistent with 0.44(2) for our ρ_6^A. Their ρ's lie in different lattice representations from all of ours, but our results indicate that this is not important. In short, the march of time has simply reduced the statistical error bars by a significant factor, and the analysis has become more sophisticated, allowing us to estimate systematic errors.

IX. $18^3\times 42$ LATTICES AT $\beta=6.2$

The data presented here are from a new analysis using the background gauge configurations of Ref. 2. Whereas

TABLE VII. Meson spectrum for $\beta=6.2$ on $18^3\times 42$ lattices. A dash indicates that no reliable fit can be made.

m_q \ fit	π 14–26	χ^2/N_{DF}	π_3 14–26	χ^2/N_{DF}	ρ_6^A 10–20	χ^2/N_{DF}
0.03	0.355(2)	15/9	0.369(2)	8/9	0.429(6)	31/7
0.03+0.02	0.328(2)	18/9	0.337(2)	6/9	0.41(1)	29/7
0.02	0.293(3)	18/9	0.302(3)	5/9	0.38(1)	24/7
0.02+0.01	0.257(4)	17/9	0.266(4)	8/9	0.36(1)	15/7
0.01	0.215(4)	19/9	0.228(5)	10/9	0.33(2)	11/7
0.01+0.007	0.201(5)	12/9	0.213(6)	8/9	-	
0.007	0.182(5)	13/9	0.197(8)	8/9	-	

previously we used antiperiodic boundary conditions and point sources for the quark propagators, we now use Dirichlet BC and wall sources. The wall sources are placed at $t=3$ and 37, and the number of lattices used varies from 28 to 32 depending on the channel.

The 18^3 lattices have the smallest physical volume of any we consider in this paper. The lattice spacing decreases between $\beta=6$ and $\beta=6.2$ by about a factor of 0.8.[2] Thus the lattice is about $0.8\times 18/16=0.9$ times smaller along a side than the 16^3 lattice at $\beta=6$. On the basis of our results at $\beta=6$, we do not expect the pion and ρ masses to be much affected by this small volume, but we cannot rule out an effect on the baryon masses.

Our results for hadron masses are given in Tables VII and VIII. We use a larger range of physical quark masses than at $\beta=6$. Using a scaling factor of 0.8, and ignoring anomalous dimensions, our range of 0.007–0.03 corresponds to 0.0087–0.0375 at $\beta=6$. Unfortunately, we gain little by going to lighter-quark masses, since the statistical errors increase rapidly in all but the pion channels.

For the pions, we only have results for π and π_3 and we quote results from the LT operators for the same reasons as at $\beta=6$. The fits are reasonable, leading to errors comparable to those at $\beta=6$. Changing the time range alters the central values by up to 2σ, the largest changes being for the heavier-quark masses.

We use the same ρ channel as before, the other channels again giving consistent masses. The fits are reasonable at the lightest masses, but get poorer as the mass increases. To see what is happening we show in Fig. 10 the ρ_6^A correlator at $m_q=0.0085$ and 0.025. The plateau is very long at $m_q=0.025$, but undulates after $t=16$, so that in our fitting range ($t=10$–20) the plateau is not very flat. For $m_q<0.01$, we do not find a convincing plateau, as illustrated in the Fig. 10, and we do not quote a ρ mass.

For the nucleons, we quote results for the operator local in time (LT), and adjust the time ranges to agree with the length of the plateau. All fits give reasonable χ^2/N_{DF}, and different time ranges give values agreeing within $\sim 1\sigma$. The NLT operator gives results 2σ higher for the heaviest masses, though the fits have a much larger χ^2, but gives consistent results with better χ^2 for the lighter-quark masses. The quality of the data is shown in Figs. 11(a) and 11(b).

Finally, we quote a result for the Δ. We find a reasonable signal in the pure Δ channel discussed in Sec. III. Figures 12(a) and 12(b) show this signal for $m_q=0.01$ and 0.03, respectively. At the heavier mass there is a clear plateau from $t=8$–16, while for the lighter mass the plateau is less convincing. Table VIII gives the results of a fit to $t=8$–16 for $m_q\geq 0.01$, the signal at lower masses being too poor to warrant fitting. Clearly, the statistical significance of $m_\Delta - m_N$ decreases as m_q decreases.

TABLE VIII. Baryon spectrum for $\beta=6.2$ on a $18^3\times 42$ lattice. A dash indicates that no reliable fit can be made.

m_q	m_N	Fit	χ^2/N_{DF}	m_Δ	Fit	χ^2/N_{DF}
0.03+0.03+0.03	0.65(1)	12–24	8/9	0.72(2)	8–16	8/9
0.02+0.03+0.03	0.63(1)	12–24	7/9	0.70(2)	8–16	6/7
0.02+0.02+0.03	0.61(1)	12–24	5/9	0.67(2)	8–16	6/7
0.02+0.02+0.02	0.58(1)	12–24	5/9	0.65(2)	8–16	5/7
0.01+0.02+0.02	0.56(1)	12–24	2/9	0.63(2)	8–16	2/5
0.01+0.01+0.02	0.54(2)	10–22	4/9	0.62(2)	8–16	2/5
0.01+0.01+0.01	0.52(2)	10–20	7/7	0.60(2)	8–16	1/5
0.007+0.01+0.01	0.52(2)	10–20	10/7	-		
0.007+0.007+0.01	0.51(2)	10–18	8/5	-		
0.007+0.007+0.007	0.51(3)	10–18	10/5	-		

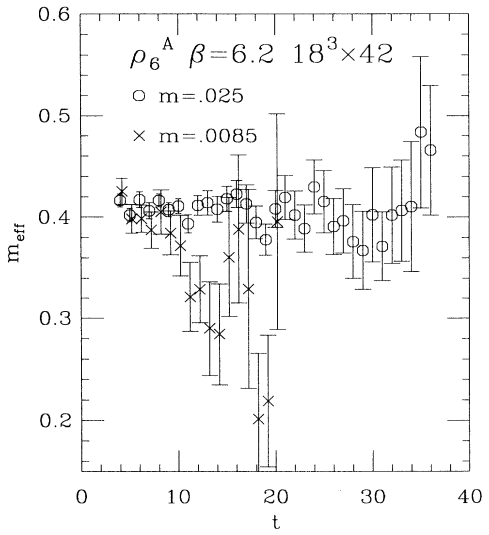

FIG. 10. Effective mass plot for the ρ_6^A on the $18^3\times42$ lattices at $\beta=6.2$ for $m_q=0.025$ (0.02+0.03) and 0.0085 (0.007+0.01). A slight horizontal offset has been added to the latter points. The wall source is at $t=3$, and the lattice ranges from $t=0$ to 41.

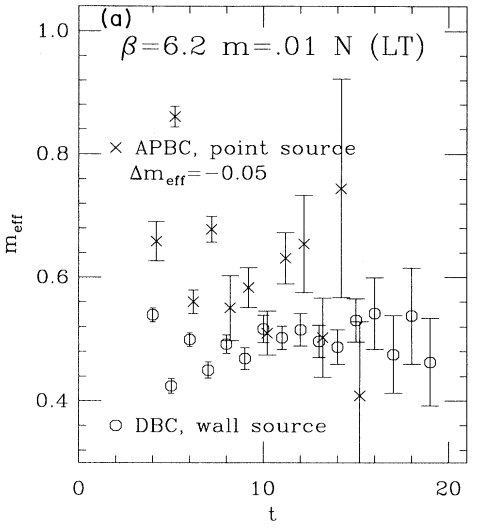

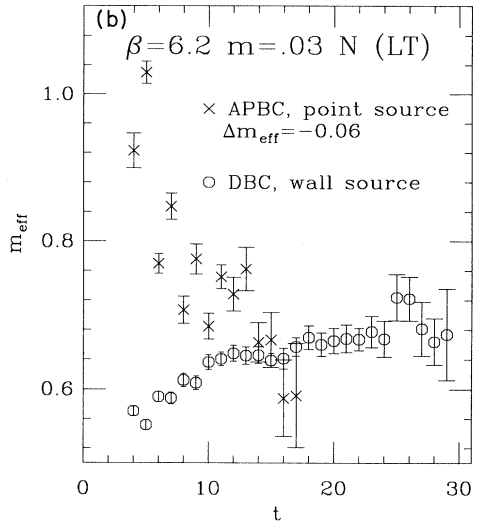

FIG. 11. Effective mass plots for nucleon, using the LT operator, on the $18^3\times42$ lattices at $\beta=6.2$. Open circles show the results from the present data set, crosses the results from Ref. 2. The latter have been shifted vertically by Δm_{eff} to remove the kinetic energy, as explained in the text. (a) $m_q=0.01$ with $\Delta m_{eff}=-0.05$. (b) $m_q=0.03$ with $\Delta m_{eff}=-0.06$.

It is interesting to compare the data at $\beta=6.2$ with those from the $16^3\times40$ lattices at $\beta=6$. The two lattices have a similar physical size, and the statistics are comparable. The data at $\beta=6.2$ is clearly better at the heavier quark masses. The quark masses in Figs. 10(a) and 10(b) (0.0085 and 0.025) are chosen so that the data for ρ can be compared with the results from $\beta=6$ shown in Figs. 4(a) ($m_q=0.01$) and 4(b) ($m_q=0.03$), respectively, if we use a scaling factor of 0.8. For the heavier masses, the signal at $\beta=6.2$ extends much further and has smaller errors. At the lighter mass, the two signals are comparable. The improved quality of the nucleon signal is also clear from a comparison of Figs. 12(a) and 12(b) with Figs. 4(a) and 4(b), respectively. (Here the matching of masses is not exact.) We discuss the comparison of the results for masses in the following two sections.

We now turn to a comparison with our earlier published results.[2] We can directly compare only the Goldstone pion, the $\tilde{\pi}$ and the nucleon, although we expect that the ρ_6^A will be nearly degenerate to the two ρ's calculated in Ref. 2. Comparing to Table II of Ref. 2 we find good agreement for both pions, while the old values for m_ρ lie consistently $\sim2\sigma$ above our new values. The differences are much larger for nucleons (Table IV of Ref. 2), the old values lying 4–5σ above our new results at the higher masses.

We have reanalyzed our old data with the improved method. Our overall conclusion is that the use of correlated errors has little effect on the extracted masses, but does increase the estimated errors in the masses, particularly for the nucleon. More importantly, we find that our old results have an additional error due to the choice of fitting range. We can reproduce our old results, but the result of varying the range changes the parameters by amounts which are much larger than the statistical error. We have remarked above that the same type of error afflicts our present data, but the error is much more severe for our old results. In fact we find, on examination of plots of m_{eff}, that the quality of the old data is very poor compared to that of the present work. In many channels the signal is so poor that we would now consider it unreasonable to do a fit.

To illustrate these comments, we show a comparison of m_{eff} for various channels. This comparison also allows us to study the efficacy of the wall sources compared to the point sources which we used in our old work. Figures 11(a) and 11(b) show the comparisons for the nucleon, us-

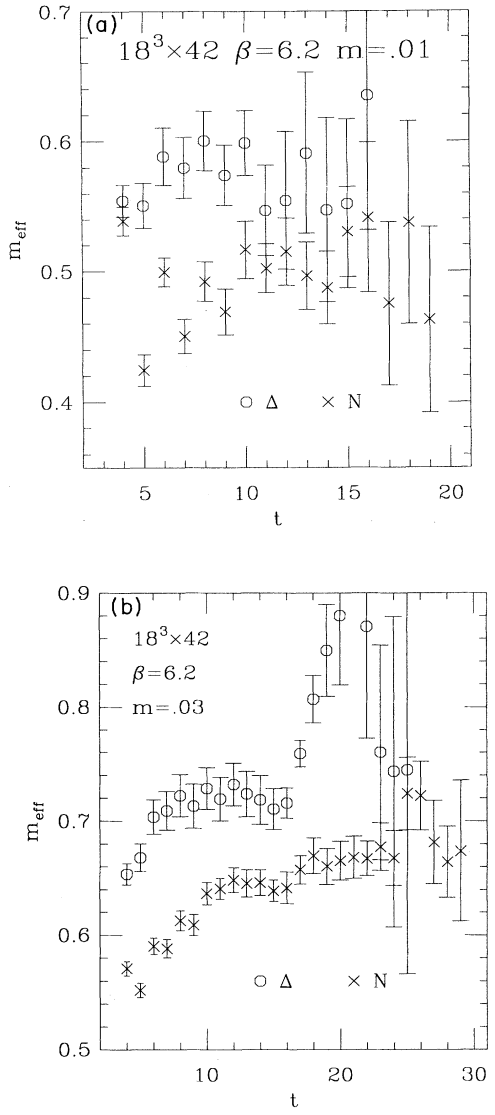

FIG. 12. Effective mass plot comparing the nucleon and Δ signals on $18^3\times42$ lattices at $\beta=6.2$, with (a) $m_q=0.01$, and (b) $m_q=0.03$.

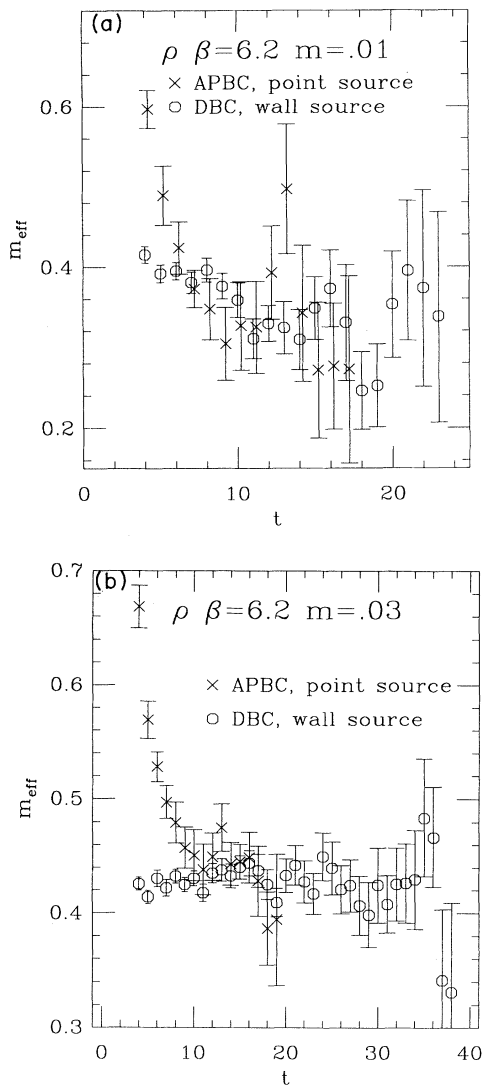

FIG. 13. Effective mass plot for the ρ's on the $18^3\times42$ lattices at $\beta=6.2$. Open circles show the results from the present data set (ρ_6^A), crosses the results from Ref. 2 using the NLT-NLT correlator. A slight horizontal offset has been added to the latter points. (a) $m_q=0.01$, and (b) $m_q=0.03$.

ing LT operators, at $m_q=0.01$ and 0.03, respectively. In Ref. 2 we used APBC in space, so that the lightest nucleon has a nonzero momentum in all three directions. We have taken the extra kinetic energy into account, following Table IV of Ref. 2, by subtracting 0.06 and 0.05, respectively, from $m_{\rm eff}$ of our old data. The use of APBC in time means that we know $m_{\rm eff}$ for only one-half the lattice.

At the heaviest mass [Fig. 11(b)], the difference in quality of the signal is enormous. The wall source reduces the transients and the statistical errors. Furthermore, the open boundary conditions allow us to follow $m_{\rm eff}$ to much longer times. As for the resulting value of m_N, our old value of 0.73(2) comes from points $t=8$–13, which from the $m_{\rm eff}$ plot one sees is not asymptotic. Our new value is 0.65(1). Similar comments apply at $m_q=0.01$ [Fig. 11(a)], except that the new signal is now less impressive. Our old value was 0.59(3), while our new result is 0.52(2). These differences between the two analyses are important, since they lower the ratio m_N/m_ρ towards the expected values, as we discuss further in the final section.

Figures 13(a) and 13(b) show the same comparison for the ρ's. The same overall comments apply as for the nucleons, except that here the old data do have a small plateau. This plateau is in good agreement with that of our new results.

Finally, we quoted, in Table III of Ref. 2, results for even-parity meson masses, whereas we do not have good signals in these channels in the present study. In Fig. 14 we show the old signal at $m_q=0.01$ for the $\tilde{\epsilon}$, for which our old result was $m=0.24(9)$. The signal is clearly unreliable. Looking at plots of $m_{\rm eff}$ in all the 0^{++}, 1^{++}, and

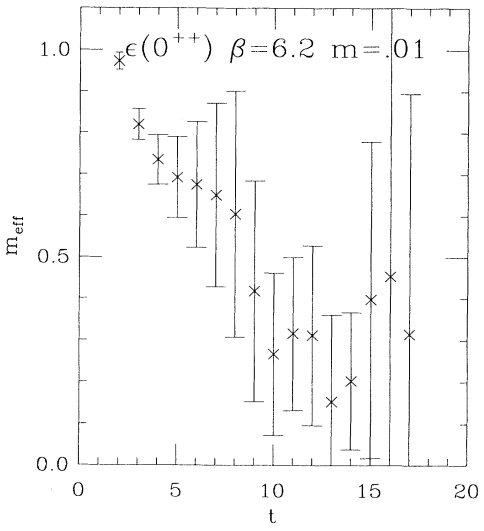

FIG. 14. Effective mass plot showing data from Ref. 2 for the $\tilde{\epsilon}$. The lattice size is $18^3\times 42$ at $\beta=6.2$ and for $m_q=0.01$.

1^{+-} channels we conclude that the results of Table III in Ref. 2 should be discarded except for those at the heaviest mass. This provides a simple solution to the problem of the $\tilde{\epsilon}$ being too light.

X. f_π, $\langle\bar{\chi}\chi\rangle$, THE LATTICE SPACING a, AND m_s

We collect together in this section various results which are related to the estimation of the lattice spacing, and to its variation with β.

The calculation of f_π is made more difficult by our use of wall sources. To extract the amplitude with which the local operator creates the pion, we need to know the coupling of the wall source to the pion. For this we must use a diagonal correlator in which the pion is destroyed by the same extended operators on a time slice which is the same distance from the boundary as the wall source (and in the same gauge). Thus, if the wall source lies on the boundary time slice (as on the lattices at $\beta=5.7$ and 6), the signal must propagate across the entire lattice.

In the following discussion we assume for definiteness that the wall source is at $t=0$, and the sink time slice is at time $T=N_t-1$. The diagonal correlator we calculate is

$$C_{WW}=\langle W|qq|\pi\rangle\langle\pi|qq+oo|W\rangle\frac{\exp(-m_\pi T)}{2m_\pi V}\ , \qquad (10.1)$$

where V is the spatial volume, and W refers to the complicated state that the wall operator acts upon. We have assumed that only the pion intermediate state (at $\mathbf{p}=0$) contributes since the correlator runs across the entire lattice. Note that we actually use the operator qq to destroy the state, but since W is a singlet under staggered fermion flavor transformations, the matrix element of oo will be the same, so we can replace qq with $(qq+oo)/2$. To extract f_π we combine C_{WW} with the wall to local correlator

$$C_{WL}(t)=\langle 0|\mathcal{O}(t)|\pi\rangle\langle\pi|qq+oo|W\rangle\frac{\exp(-m_\pi t)}{2m_\pi V}\ , \qquad (10.2)$$

where we have taken t large enough that the pion dominates, but not too large that boundary effects become important. The operator $\mathcal{O}=\bar{\chi}(n)\chi(n)(-1)^n$ is the completely local pion operator residing on a single site, in terms of which f_π is given by[8]

$$f_\pi=\frac{m_q|\langle\pi|\mathcal{O}|0\rangle|}{\sqrt{2}m_\pi^2}\ . \qquad (10.3)$$

With staggered fermions, there are no perturbative correction factors to this formula. Combining Eqs. (10.1), (10.2), and (10.3), we obtain f_π. We actually use a hypercube operator residing on two time slices, and summed over spatial positions, but this is easily accounted for.

The results for $\beta=6$ on the two lattices sizes are shown in Fig. 15, together with a linear fit to the 24^3 data. The two lattice sizes give results consistent within the errors. Our results disagree at about the 2σ level with those from Ref. 25 which quotes $f_\pi=0.067$ at $m_q=0.04$ and $f_\pi=0.051$ at $m_q=0.01$. These results use point sources on $16^3\times 32$ lattices with antiperiodic boundary conditions in space, and Dirichlet boundary conditions in time. The source is four time slices from the boundary, which they assume is sufficient to eliminate boundary effects. On the basis of our results for the pion propagator, as illustrated in Fig. 5, we would claim that at least 10 time slices are needed to remove boundary effects. Thus it is likely that the results of Ref. 25 suffer from boundary effects.

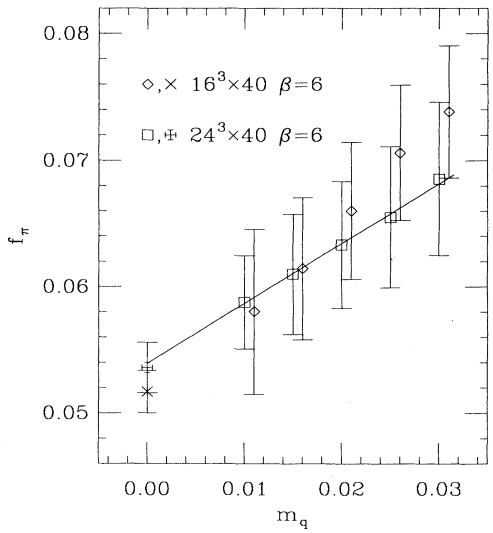

FIG. 15. Results for f_π (in lattice units) from $\beta=6$. The points from the 16^3 lattice have been offset horizontally for clarity. The results at nonzero m_q come from the amplitude of the pion correlators, and the line shows a linear fit to the 24^3 results. The points at $m_q=0$ use $\langle\bar{\chi}\chi\rangle$ extrapolated to $m_q=0$.

We can also calculate f_π using the condensate extrapolated to zero quark mass:

$$f_\pi(m_q=0)=\left[\frac{m\langle\bar{\chi}\chi(m_q=0)\rangle}{2m_\pi^2}\right]^{1/2}. \tag{10.4}$$

We cannot use wall sources to calculate $\langle\bar{\chi}\chi\rangle$, but, as part of our weak matrix element calculations, we do have available a noisy estimator of $\langle\bar{\chi}\chi\rangle$. We calculate $\phi_i=(\not{D}+m)^{-1}\eta_i$, where $\{\eta_i\}$ is a sample of a Gaussian noise vectors, and then use $\langle\bar{\chi}\chi(n)\rangle=\langle\langle m\bar{\phi}(n)\phi(n)\rangle\rangle$, where the average is over the pseudofermions ϕ_i. We have done 24 pseudofermion inversions on each lattice at each mass. We have also calculated, using source methods, a noisy estimator of the derivative $d\langle\bar{\chi}\chi\rangle/dm$. The noise in the estimator is balanced by the fact that we have a value for every site. To illustrate the quality of the results, we show in Fig. 16 the condensate averaged over each time slice, for $m_q=0.01$ on the large lattice. The boundary effects (extending for about 10 time slices) are clear, as well as the plateau region in the center. To quote numbers we use the results from $t=20$.

To extrapolate $\langle\bar{\chi}\chi\rangle$ to $m_q=0$, we follow Ref. 2 and calculate the intercept

$$\mathrm{Int}(m_q)=\left[1-m\frac{d}{dm}\right]\langle\bar{\chi}\chi\rangle. \tag{10.5}$$

Figure 16 also shows $md\langle\bar{\chi}\chi\rangle/dm$, the quantity to be subtracted from $\langle\bar{\chi}\chi\rangle$ to obtain the intercept. The results for the condensate and the intercept on the $\beta=6$ lattices are shown in Fig. 17. Also shown are linear fits to the condensate, and fits of the form $A+Bm_q^2$ to the intercept. We use the latter to extract $\langle\bar{\chi}\chi\rangle(m_q=0)=0.033$ and 0.029 on the 24^3 and 16^3 lattices, respectively, with errors in both cases ~ 0.002. Thus there is a possible 2σ finite-size effect. We can again compare our results with

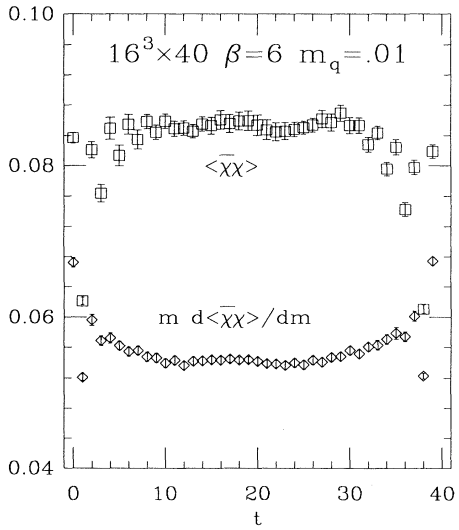

FIG. 16. Results for $\langle\bar{\chi}\chi\rangle$, averaged over each time slice, and for $md\langle\bar{\chi}\chi\rangle/dm$. The lattice size is $16^3\times40$, with $\beta=6$ and $m_q=0.01$.

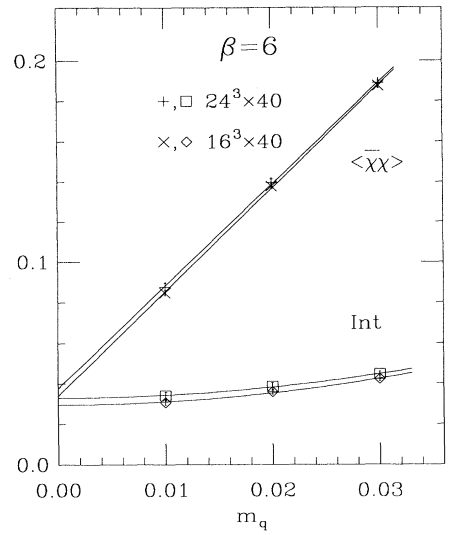

FIG. 17. Results for $\langle\bar{\chi}\chi\rangle$ and $\mathrm{Int}(m_q)$ at $\beta=6$. Also shown are linear fits to the condensate, and fits of the intercept to $A+Bm_q^2$.

those of Ref. 25. They find an extrapolated value for $\langle\bar{\chi}\chi\rangle$ of 0.036, with an estimated 20% error, which is consistent with our result. For the intercept, however, they find 0.024 at $m_q=0.01$, considerably below our value of 0.031(1), and even further below their extrapolated value for $\langle\bar{\chi}\chi\rangle$. They attribute this low result to the use of too small quark masses. In fact, it is clear from Fig. 16 that the discrepancy could easily be due to the boundary effects, which reduces the intercept below its value in the plateau.

With our extrapolated condensate in hand, we can use Eq. (10.4) to calculate f_π directly at $m_q=0$. The results for the two lattice sizes are shown as points at $m_q=0$ in Fig. 15. The agreement with the result from extrapolating f_π directly (the solid line) provides a check on our extraction of $f_\pi(m_q)$.

Linear fits to f_π extracted using the amplitude of the correlators give

$$\begin{aligned} f_\pi&=0.118(7)+0.97m_q \quad \text{at } \beta=5.7\ ,\\ f_\pi&=0.054(5)+0.47m_q \quad \text{at } \beta=6.0\ (24^3\times40)\ ,\\ f_\pi&=0.032(4)+0.45m_q \quad \text{at } \beta=6.2\ . \end{aligned} \tag{10.6}$$

At $\beta=6.0$, the result from the condensate is $f_\pi(m_q=0)=0.054(2)$. The result at $\beta=6.2$ is in agreement with our previous estimate,[2] using the condensate, of $f_\pi(m_q=0)=0.035(1)$.

We now turn to our determinations of the lattice spacing. We obtain three estimates using $m_\rho(m_q=0)$, $m_N(m_q=0)$, and $f_\pi(m_q=0)$. In addition, the ratio of the slopes, $R=A_\pi/A_\rho$, can be determined if we assume $m_\rho=A_\rho m_q+B_\rho$ and $m_\pi^2=A_\pi m_q+B_\pi$. Comparing with experimental value of

$$R=\frac{m_K^2-m_\pi^2}{m_K^*-m_\rho}$$

TABLE IX. Various determinations of the scale. The $\beta=6$ results are from the $24^3\times 40$ lattice. A dash indicates that no result is available.

Scale M	Expt. (GeV)	$\beta=5.7$ $aM(m_q=0)$	$\beta=5.7$ a^{-1} (GeV)	$\beta=6$ $aM(m_q=0)$	$\beta=6$ a^{-1} (GeV)	$\beta=6.2$ $aM(m_q=0)$	$\beta=6.2$ a^{-1} (GeV)
m_ρ	0.770	0.78(7)	1.0(1)	0.410(15)	1.9(1)	0.29(1)	2.7(1)
m_N	0.938	-		0.490(16)	1.9(1)	0.45(2)	2.1(1)
f_π	0.093	0.118(7)	0.8(1)	0.054(2)	1.7(1)	0.032(4)	2.9(4)
R	1.87	-		1.15(12)	1.6(2)	0.87(11)	2.1(3)

gives a fourth independent estimate. These estimates are collected in Table IX.

At $\beta=6$ there is good consistency in the determination of the scale. The range $a^{-1}=1.6$–1.9 GeV agrees with previous determinations. The results at $\beta=6.2$ are consistent with those from our previous work.[2] As before, the most significant discrepancy is the familiar disagreement between the nucleon and ρ scales, which we discuss further below. Asymptotic scaling, at the two-loop level, predicts that $a(\beta=6.2)\approx 0.8a(\beta=6)$. We find the ratios in rough agreement with this prediction: 0.7, 0.9, 0.6, and 0.8 for the four quantities in the table. At $\beta=5.7$ we find $1/a\sim 1$ GeV from both m_ρ and f_π, though we have no results from the other methods. The ratio of the scale at $\beta=6$ to that at $\beta=5.7$ (a factor of ~ 2) is greater than the factor of 1.4 predicted by asymptotic scaling. These conclusions on scaling agree qualitatively with those of Ref. 25.

Having determined the lattice scale we can extract values for m_s. We do this using the experimental values for m_{K^*}/m_K, m_{K^*}/m_ρ, m_K/m_ρ, and m_K/f_π. In the latter case, for example, we adjust the quark mass until the ratio of the lattice m_π to the lattice value of $f_\pi(m_q=0)$ equals the continuum ratio m_K/f_π. This then corresponds to $m_q=m_s/2$. For $\beta=5.7$ the different methods give completely inconsistent answers, since there is little resemblance between lattice and physical spectra. For $\beta=6$ the results lie in the range $m_s a=0.024$–0.029. Converting to physical units using the same quantity to set the scale as is used to determine m_s, we find $m_s=46$–49 MeV. For $\beta=6.2$, we find $m_s a$ ranging from 0.012 to 0.020, with $m_s=35$–54 MeV. This is consistent with our previous results,[2] as well as with the value at $\beta=6$.

These results are quite different from continuum estimates. At a scale of ~ 2 GeV, which is similar to the scale of the lattice evaluation, $m_s^{\rm cont}\sim 150$ MeV.[26] This is ~ 3 times larger than the lattice value, much larger than can be accounted for by perturbative corrections.[27] [An essentially equivalent way of stating the discrepancy is that the continuum condensate $\langle\bar{u}u\rangle\approx 0.0114$ GeV^3 (Ref. 26) is roughly three times larger than the lattice result $(\langle\bar{\chi}\chi\rangle/4)^{-1/3}=0.038(3)$, where the factor of 4 accounts for the number of flavors.] We have suggested before[28] that this discrepancy may be due to the use of the quenched approximation. If we fix the scale with f_π, and use m_K/f_π to fix m_s, then, since the lattice and continuum pseudoscalar masses are consistent with $m_\pi^2 f_\pi^2=m_q\langle\bar{u}u+\bar{d}d\rangle$, we are in effect fixing $m_s\langle\bar{\chi}\chi\rangle(m_q=0)$ to its physical value. But we expect $\langle\bar{\chi}\chi\rangle$ to be too large in the quenched approximation, since configurations which have small eigenvalues, and which therefore give large contributions to $\langle\bar{\chi}\chi\rangle$, are not suppressed by the determinant. Thus we expect m_s to be too small. Runs on lattices similar to ours, but including dynamical fermions, show at most a small (nowhere near a factor of 2) effect on the condensate.[29] However these runs have been done with quark masses near the strange-quark mass, and it is quite plausible that the mechanism we describe will only take effect when effects of the lighter up and down quarks are taken into account.

It is interesting to note that the quark masses that one finds with Wilson fermions are heavier than those for staggered fermions.[4] The ratio of Wilson to staggered masses is roughly 3 at $\beta=6$, and ~ 2 at $\beta=6.2$. There are considerable uncertainties in these numbers, but it is clear that the difference between continuum and Wilson fermion quark masses is much smaller than for staggered fermions.

Finally, we can use our values for m_s to estimate the lattice result for f_K/f_π. At $\beta=6$ we find 1.21–1.25, while for $\beta=6.2$ we have 1.16–1.28, where the ranges are due to the uncertainty in m_s. Since the quenched approximation does not include pion and kaon loops, the quenched answer may differ from the continuum value of 1.22 by ~ 0.1.[30] Thus our result can only be considered a qualitative, and not a quantitative, success.

XI. COMPARISONS

We now turn to comparisons between the spectrum at $\beta=6.0$ and 6.2, and between our results and those obtained using Wilson fermions. Both comparisons are aimed at testing the approach to the scaling limit.

In Fig. 18 we show the π,π_3,ρ, and nucleon masses plotted against m_q. Figure 18(a) shows the results for the large lattice at $\beta=6$. Figure 18(b) shows results from $\beta=6.2$ rescaled by a factor of 0.8 to take into account the difference in lattice scales. The dashed lines show the fits to the data displayed in Fig. 18(a). The Goldstone-pion data agree well, and the trend towards flavor-symmetry restoration is very clear. There are, however, clear signs of scaling violations in the ρ masses, and in the slope of the nucleon data.

Flavor-symmetry breaking gives rise to a difference in slope ($A_\pi\neq A_{\pi_3}$) and in intercept between Goldstone and non-Goldstone pions. Only the slopes have small enough errors that we can study the dependence on lattice spac-

ing. We expect that the quantity $\delta=(A_{\pi_3}-A_\pi)/A_\pi$ will vanish as a power of a in the continuum limit. This ratio is an attractive object to study because anomalous dimension factors from the quark mass cancel. We find this quantity to be 0.07 and 0.04, for $\beta=6$ and 6.2, respectively, with poorly determined errors of at least 0.01 in both cases. Recall that we find the ratio of lattice spacings to be 0.6–0.9 (see the previous section). Thus, all we can say is the symmetry breaking is decreasing as the continuum limit is approached, but we cannot distinguish between a linear and a quadratic dependence on a.

To investigate the β dependence of ρ and nucleon masses we show in Fig. 19 the dimensionless ratio m_N/m_ρ on the APE plot. The errors have been obtained using the jackknife method. The squares are the experimental point and that for $m_q=\infty$. The two solid lines are estimates of how the mass ratio is expected to behave as a function of the quark mass, and are meant to serve as a rough guide. For further discussion, see Refs. 4 and 31. Results are given for the large lattice at $\beta=6$, and from $\beta=6.2$. For the baryons, we use LT operators.

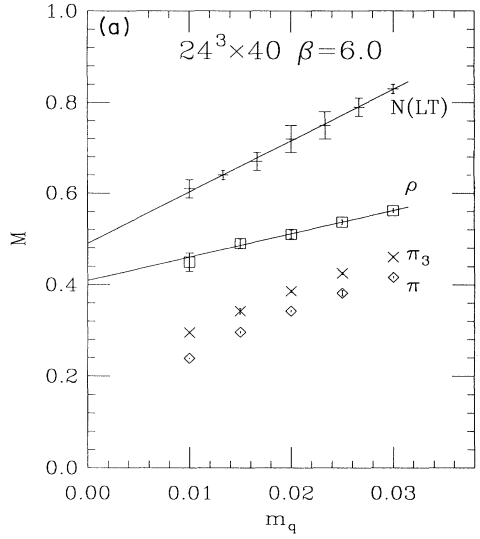

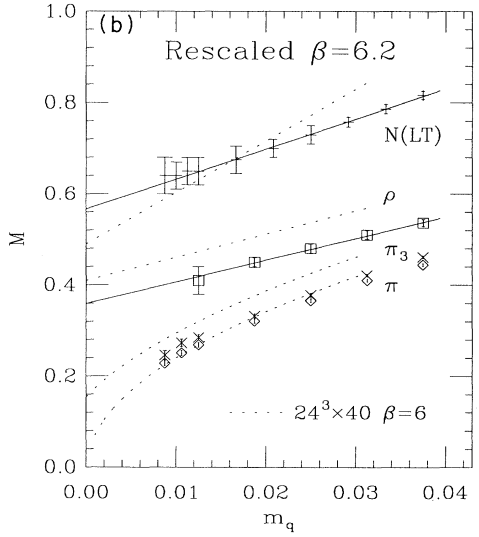

FIG. 18. The spectrum as a function of the quark mass. The solid lines are linear fits. (a) Results from $\beta=6$ on $24^3\times40$ lattices, using the LT nucleon operator, and the fits to $t=15$–25 for the pions. (b) Rescaled results (using a factor of 0.8) from $\beta=6.2$ on $18^3\times42$ lattices. The dashed lines are the fits to the $\beta=6$ data shown in (a), with quadratic fits used for the pions.

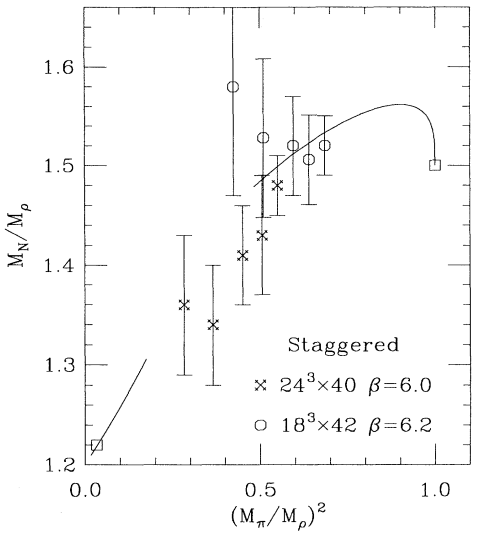

FIG. 19. Staggered fermions APE plot for the mass ratio m_N/m_ρ, using the LT nucleon operator, and the fits to $t=15$–25 for the pions at $\beta=6$. Extra points have been added by interpolating the baryon results.

Our most reliable results are on the large lattice at $\beta=6$. These are consistent with the solid curves, actually falling below rather than above. Although the errors are too big to do a reasonable extrapolation, it is worth emphasizing that there is no reason why the quenched results should not extrapolate to a value below the experimental point.[32] It is gratifying, however, to find results for m_N/m_ρ which are decreasing as the quark mass decreases. The only caveat is that, as discussed above, there may be a small residual finite-size shift in the nucleon mass.

Unfortunately, this happy situation does not hold at $\beta=6.2$. Although our new results for m_N/m_ρ are considerably lower than those in Ref. 2, they still deviate from the large lattice $\beta=6$ results at small m_q. Given the large systematic uncertainties in fitting, the size of the statistical errors at $\beta=6.2$, and the possibility of finite-size effects in the nucleon mass, we cannot, however, draw any definite conclusions about scaling. Clearly what we need are better statistics at $\beta=6$, and a new calculation at $\beta=6.2$ on a larger lattice.

We can compare our results on the 24^3 lattice at $\beta=6.0$ with a calculation using $24^3\times32$ lattices carried out by the APE group using Wilson fermions.[33] Figure 20 shows the APE plot for Wilson fermions. The mass ratios at $\beta=6$ are in reasonable agreement with those for staggered fermions shown in Fig. 19. Scaling violations

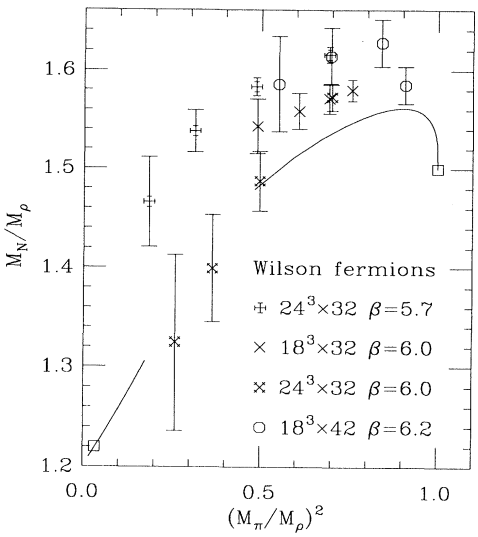

FIG. 20. Wilson fermions APE plot. The data at $\beta=5.7$ and that at $\beta=6$ is from Ref. 33 and that at $\beta=6.2$ from our previous work (Ref. 2).

do appear, however, if we make a more detailed comparison. We do this by matching the pion masses of the two fermion formulations, and comparing the ρ and nucleon masses. We compare using both the staggered Goldstone pion and one of the non-Goldstone pions since there is no *a priori* reason for choosing one over the other. Table X(a) shows the comparison using the Goldstone pion. The staggered ρ and nucleon masses lie significantly above those for Wilson fermions. The agreement is much improved if we match using the staggered $\tilde{\pi}$, as shown in Table X(b).

TABLE X. (a) Comparison of the spectrum for staggered and Wilson fermions at $\beta=6.0$ on 24^3 lattices. We use the LT nucleon operator, and have interpolated to get a value for staggered fermions at $m_q=0.01+0.02$. (b) same as for (a), except matching the staggered $\tilde{\pi}$ with the Wilson fermion pion.

(a)

Mass	π	ρ	Nucleon
$m_q=0.03+0.03$	0.417(2)	0.562(4)	0.83(1)
$\kappa=0.1530$	0.422(2)	0.504(4)	0.793(8)
$m_q=0.01+0.02$	0.296(2)	0.49(1)	0.65(2)
$\kappa=0.1550$	0.298(2)	0.423(7)	0.629(13)
$m_q=0.01+0.01$	0.239(2)	0.45(2)	0.61(2)
$\kappa=0.1558$	0.236(3)	0.392(11)	0.549(19)

(b)

Mass	$\tilde{\pi}$	ρ	Nucleon
$m_q=0.02+0.03$	0.417(4)	0.537(5)	0.77(2)
$\kappa=0.1530$	0.422(2)	0.504(4)	0.793(8)
$m_q=0.01+0.01$	0.295(3)	0.45(2)	0.61(5)
$\kappa=0.1550$	0.298(2)	0.423(7)	0.629(13)

TABLE XI. Comparison of the spectrum for staggered and Wilson fermions at $\beta=6.2$ on 18^3 lattices. The data at $\kappa=0.32$ and 0.325 are with $r=0.5$ Wilson fermions. A dash indicates that no result is available.

Mass	π	ρ	Nucleon
$m_q=0.03$	0.355(2)	0.429(6)	0.653(7)
$\kappa=0.151$	0.358(5)	0.416(1)	-
$\kappa=0.320$	0.37(1)	0.443(6)	0.715(8)
$m_q=0.02$	0.293(3)	0.38(1)	0.58(1)
$\kappa=0.152$	0.300(6)	0.368(2)	-
$\kappa=0.325$	0.29(1)	0.39(1)	0.62(1)
$m_q=0.01$	0.215(4)	0.33(2)	0.52(2)
$\kappa=0.152$	0.224(9)	0.322(6)	-

At $\beta=6.2$, we can compare with our old $r=1/2$ Wilson fermion results from the same lattices.[2] In addition, for $r=1$ Wilson fermions, there exists data on $16^3\times40$ lattices for the pion and ρ from the ELC Collaboration.[34] In Table XI we compare the spectra, again fixing quark masses so that the pion masses agree. (Here the difference between π and $\tilde{\pi}$ is too small to be important.) The pattern is similar to that at $\beta=6$ when using $\tilde{\pi}$ to do the matching [see Table X(b)].

XII. CONCLUSIONS

The size of staggered flavor-symmetry breaking and the lack of signal in ρ and nucleon correlators at $\beta=5.7$ mandates that future calculations be done at $\beta\geq6.0$, with $\beta\geq6.2$ preferable.

To do such calculations efficiently, extended sources are mandatory. We use a wall source, and find that the improvement in the quality of the signal in hadron correlators is similar to that obtained using the APE cube sources. A particularly useful feature of our source is that it allows us to study a number of pion and ρ representations, while generating states with zero momentum. In addition, the sources also produce the Δ, and we find a reasonable signal for this particle at $\beta=6.2$. To the best of our knowledge, this is the first time that a signal for the Δ has been obtained using staggered fermions.

We do not find a signal in the even-parity meson sector on any of the lattices considered in this study. A reanalysis of the data given in Table III of Ref. 2 indicates that those results should be discarded, except at the heaviest-quark mass. In particular, there is no evidence for an anomalously light scalar.

At $\beta=6$ our results show that finite-size effects in pion and ρ masses are small or absent on a 16^3 lattice. For the baryons, however, there are contradictory indications, and all we can do is limit possible finite-size effects. For our two lattice sizes, the difference in the nucleon mass at small quark masses is 10% or less. It would be useful to improve the statistical precision of these results in order to determine the minimum volume one can safely use for a nucleon at rest.

The results on the 24^3 lattice at $\beta=6.0$ probably represent, within the statistical and systematic errors discussed above, infinite-volume results. We find that the ratio m_N/m_ρ lie considerably below previous results using staggered fermions, and there is encouraging agreement with Wilson fermions. Nevertheless, a glance at Figs. 19 and 20 is sufficient to indicate that much work remains. To systematically investigate the validity of the quenched approximation, we have to work at weaker coupling and with smaller quark masses, and we must reduce the size of the errors.

Note added. Another sighting of the Δ baryon has been made, using techniques similar to those presented here.[35]

ACKNOWLEDGMENTS

We thank C. Bernard, T. DeGrand, A. Kronfeld, and L. Yaffe for discussions. The $\beta=5.7$ and $\beta=6.0$ studies are part of a project made possibly by the NERSC. We thank J. Mandula and T. Kitchens for their tremendous support. The $\beta=6.2$ calculations were done at Los Alamos National Laboratory. We are grateful to A. Hayes and A. White for their encouragement and support. S.R.S. was supported in part by the Outstanding Junior Investigator program through Contract No. DE-AT06-88ER40423, the Alfred P. Sloan Foundation, and by NSF Grant No. PHY89-04035 (supplemented by funds from NASA).

---

*Permanent address.

[1]See, for example, G. Kilcup, S. Sharpe, R. Gupta, and A. Patel, Phys. Rev. Lett. **64**, 25 (1990).

[2]R. Gupta, G. Guralnik, G. Kilcup, A. Patel, S. Sharpe, and T. Warnock, Phys. Rev. D **36**, 2183 (1987).

[3]K. M. Bitar *et al.*, Report No. FSU-SCRI-90-98 (unpublished).

[4]R. Gupta, in *Lattice '89,* proceedings of the 1989 Symposium on Lattice Field Theory, Capri, Italy, 1989, edited by N. Cabibbo *et al.* [Nucl. Phys. B (Proc. Suppl.) **17**, 70 (1990)].

[5]S. Sharpe, in *Hadronic Matrix Elements and Weak Decays,* proceedings of the Ringberg Workshop, Ringberg Castle, West Germany, 1988, edited by A. J. Buras, J.-M. Gérard, and W. Huber [Nucl. Phys. B (Proc. Suppl.) **7A**, 255 (1989)].

[6]G. Kilcup, in *Lattice '88,* proceedings of the International Symposium, Batavia, Illinois, 1988, edited by A. S. Kronfeld and P. B. Mackenzie [Nucl. Phys. B (Proc. Suppl.) **9**, 201 (1989)].

[7]M. F. L. Golterman, Nucl. Phys. **B273**, 663 (1986).

[8]G. W. Kilcup and S. R. Sharpe, Nucl. Phys. **B283**, 493 (1987).

[9]M. F. L. Golterman and J. Smit, Nucl. Phys. **B255**, 328 (1985).

[10]A. Billoire, R. Lacaze, E. Marinari, and A. Morel, Nucl. Phys. **B251**, 581 (1985).

[11]H. Kluberg-Stern, A. Morel, O. Napoly, and B. Petersson, Nucl. Phys. **B220**, 447 (1983).

[12]K. C. Bowler, C. B. Chalmers, R. D. Kenway, D. Roweth, and D. Stephenson, Nucl. Phys. **B296**, 732 (1988).

[13]Y. Iwasaki, in *Lattice '88* (Ref. 6), p. 254.

[14]A. Billoire, E. Marinari, and G. Parisi, Phys. Lett. **162B**, 160 (1985).

[15]F. Brandstaeter, A. S. Kronfeld, and G. Schierholz, Nucl. Phys. **B345**, 709 (1990).

[16]P. Bacilieri *et al.*, Nucl. Phys. **B317**, 509 (1989).

[17]C. Bernard, D. Murphy, A. Soni, and K. Yee, in *Lattice '89* (Ref. 4), p. 593.

[18]S. Güsken, U. Löw, K.-H. Mutter, R. Sommer, A. Patel, and K. Schilling, Phys. Lett. B **227**, 266 (1989).

[19]E. Marinari, in *Lattice '89* (Ref. 4), p. 431.

[20]P. Bacilieri *et al.*, Nucl. Phys. **B343**, 228 (1990).

[21]R. Gupta, G. Kilcup, A. Patel, S. Sharpe, and P. de Forcrand, Mod. Phys. Lett. A **14**, 1367 (1988).

[22]Ph. de Forcrand and R. Gupta, in *Lattice '88* (Ref. 6), p. 516.

[23]K. C. Bowler, C. B. Chalmers, R. D. Kenway, G. S. Pawley, and D. Roweth, Nucl. Phys. **B284**, 299 (1987).

[24]D. Barkai, K. J. M. Moriarty, and C. Rebbi, Phys. Lett. **156B**, 385 (1985).

[25]K. C. Bowler, R. D. Kenway, D. Roweth, and D. Stephenson, Nucl. Phys. **B301**, 304 (1988).

[26]J. Gasser and H. Leutwyler, Phys. Rep. **87**, 77 (1982).

[27]M. F. L. Golterman and J. Smit, Phys. Lett. **140B**, 392 (1984).

[28]S. R. Sharpe, R. Gupta, G. Guralnik, G. Kilcup, and A. Patel, Phys. Lett. B **192**, 149 (1987).

[29]H. Chen, presented at Lattice '90, proceedings, Tallahassee, Florida, 1990 (unpublished).

[30]S. Sharpe, in *Lattice '89* (Ref. 4), p. 146.

[31]S. Sharpe, presented at PASCOS-90, Boston, Massachusetts, 1990 (unpublished).

[32]A. Patel, R. Gupta, G. Kilcup, and S. Sharpe, Phys. Lett. B **225**, 398 (1989).

[33]M. Guagnelli, presented at Lattice '90 (Ref. 29).

[34]O. Pene (private communication).

[35]A. Ukawa, presented at Lattice '90 (Ref. 29).